SPECTRAL DECOMPOSITION TECHNIQUES AS HYDROCARBON INDICATORS. A CASE STUDY OF WEST WAHA AND WORSHAM BAYER FIELD, WEST TEXAS.

……..

A Thesis presented to

the Faculty of Department of Earth and Atmospheric Sciences

University of Houston

……..

In Partial Fulfillment

of the Requirements for the Degree

Master of Science

…….

By

Adebowale Michael Adekunle

May, 2012

SPECTRAL DECOMPOSITION TECHNIQUES AS

HYDROCARBON INDICATORS.

A CASE STUDY OF WEST WAHA AND WORSHAM BAYER FIELD,

WEST TEXAS.

……
Adebowale Michael Adekunle

……
Dr. John Castagna, Chairman

……
Dr. Evgeni Chesnokov, Member

……
Dr. Robert Wiley, Member

…….
Dr. Mark A. Smith
Dean, College of Natural Sciences and Mathematic

Acknowledgement

I thank God for helping through the program successfully, my sincere gratitude to my advisor and committee members, Dr. John Castagna, Dr. Evgeni Chesnokov, and Dr. Robert Wiley for their support and time. Special gratitude to my Aunty, Mrs. Olufolake Ogunsola, I wish to thank my friends; Arnold Oyem, Ayodeji Babalola, Bode Omoboya, and Doyin Pelemo. Special thanks to my father, Mr. John Adekunle and my sister for their love. I remember my grandprents, Mr. and Mrs. Osindeinde. My almost gratitude to my lovely wife, Abimbola Adekunle for been supportive all the way through thick and thin.

SPECTRAL DECOMPOSITION TECHNIQUES AS

HYDROCARBON INDICATORS

A CASE STUDY OF WEST WAHA AND WORSHAM BAYER FIELD,

WEST TEXAS.

……..

A Thesis Presented to

the Faculty of Department of Earth and Atmospheric Sciences

University of Houston

……..

In Partial Fulfillment

of the Requirements for the Degree

Master of Science

…….

By

Adebowale Michael Adekunle

May, 2012

Abstract

The frequency content of a seismogram varies with time and amplitude response to thickness and porosity in frequency domain more than in time domain, hence analysis of a time domain signal in the frequency domain shows features that are not visible on the time domain sections. The following spectral decomposition techniques: Constrained Least Square Spectral Analysis (CLSSA), Discrete Fourier Transform (DFT), and Continuous Wavelet Transform (CWT), were applied on the field data from West Waha and Worsham Bayer fields. All the techniques illuminate the reservoirs and also identify low frequency shadows beneath the reservoirs at low frequency. This validates that the recently developed CLSSA is a good direct hydrocarbon detection technique.

The application of these techniques on a horizon across a channel feature on the Stratton field dataset and comparison of the results reveal CLSSA is best for subtle structure delineation. CLSSA reveals the lateral extent of the channel branches more than DFT and CWT.

Application of these techniques on synthetic traces also reveals that CLSSA better separate events that are closely spaced without producing side lobe effects and notches as seen on the Discrete Fourier Transform (DFT). Continuous Wavelet Transform could not separate the events in time at low frequency.

Table of Contents

List of Figures

Chapter One

1.0 Introduction

This research is aimed at using different spectral decomposition techniques as hydrocarbon indicators and also comparing the techniques in terms of temporal and frequency resolution. The aim of the reservoir geophysicist in exploration and production is to detect hydrocarbon, but one of the major limiting factors faced by an interpreter is detecting thin reservoirs, especially reservoirs below seismic resolution. Chopra et al. (2006) stated that the vertical seismic resolution is the ability to distinguish two or more separate events or reflections in both time and depth domain. Widess (1973) used reflective properties to define thin beds as the bed with thickness less than $1/8^{th}$ of its wavelength. Interpreters are overwhelmed by the problem of resolution limits as thin beds with appreciable commercial hydrocarbons are left undetected. Spectral decomposition is a novel method which helps in addressing the problem of seismic resolution limit and reduce the risk involve in drilling dry well.

Partyka et al. (1999) developed spectral decomposition, a technique aimed at enhancing seismic resolution and aid interpretation of thin beds because the concept is based on the fact that thin bed reflectivity has a unique response in the frequency domain. Spectral decomposition was used for layer thickness determination (Partyka et al., 1999), Stratigraphic visualization and reservoir delineation (Marfurt and Kirlin, 2001). Castagna et al. (2003), Burnett et al. (2003), Fahmy et al. (2005), Sinha et al. (2005), Yandong et al. (2011), have all used spectral decomposition as direct hydrocarbon detection

technique in complex hydrocarbon plays.

Spectral decomposition principle assumes that the frequency content of a seismic signal varies with time. This implies that at different times, the frequency content of a seismogram is non-uniform. Thus the transformation of a signal from a time domain into a frequency domain and the analysis of the amplitude and phase spectra at each frequency enable temporal bed thickness delineation and lateral geologic discontinuities associated with each frequency (Partyka, 1999).

1.1 Geologic Setting of the Study Area.

The West Waha and Worsham-Bayer fields (West Texas) form a part of the Delaware Basin which is a sub basin of the larger Permian Basin (Keran and Holtz, 1992).

The field is principally a natural gas producing field with four gas producing units. The Ellenburger Formation contains the major producing units, while the Silurian Fusselman unit and Devonian Thirtyone unit and Mississippian limestone are minor gas producing strata (Kerans et al. 1990). Figure 1.1 shows the map of the study area.

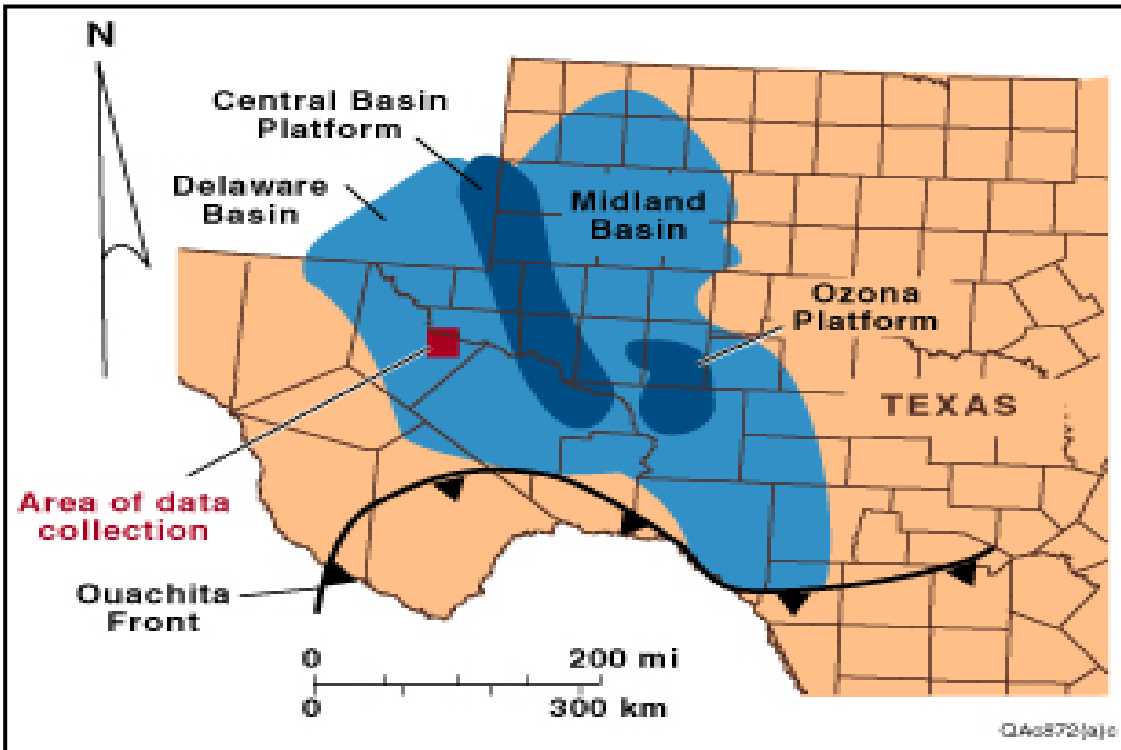

Figure 1.1: Location map of the study area. (Hardage and Hentz, 1998)

During the Paleozoic era, the stable West Texas was flooded resulting in deposition of limestone and shale. During the late Paleozoic Era, the collision of the European and African plates with North and South American plates resulted in sedimentary filling of the Ouachita Trough. Convergence of the North and South American plates resulted in faulted mountain uplifts of the Ouachita Mountains and basin filled by shallow inland sea of the West Texas (Keran and Holtz, 1992).

Cambrian rifting along southern North America margin formed broad shallow water in southern West Texas during the Ordovician. The carbonate Ellenburger sediments transgress over the basement to a thickness of 518 m. The karsting of the Ellenburger Group in middle Ordovician led to deposition of sandstones and shales of the Simpson Group (T.E Ewing, 1991). This was followed by the deposition of carbonate and

siliciclastic rocks that constitute the Montaya and Fusselman Formations, Wristen Group, and Thirtyone Formation. Woodford Formation, a shale unit and the major hydrocarbon source rock in West Texas was formed during the Late Devonian and Early Mississippian period (Lucia, F.J., 1995).

Regional tectonic deformation of the Ouachita Mountain building resulted in structural deformation in West Texas. West Texas was divided into the Delaware and Midland Basin due to uplift of the Central Basin Platform. This uplift resulted in thrust faulting, structural rotation, and strike- slip deformation in West Waha and Worsham-Bayer field. These structures serve as hydrocarbon traps for Ordovician through Mississippian reservoirs (Loucks and Anderson, 1985). Figure 1.2 shows the stratigraphy column of the Permian Basin in West Texas.

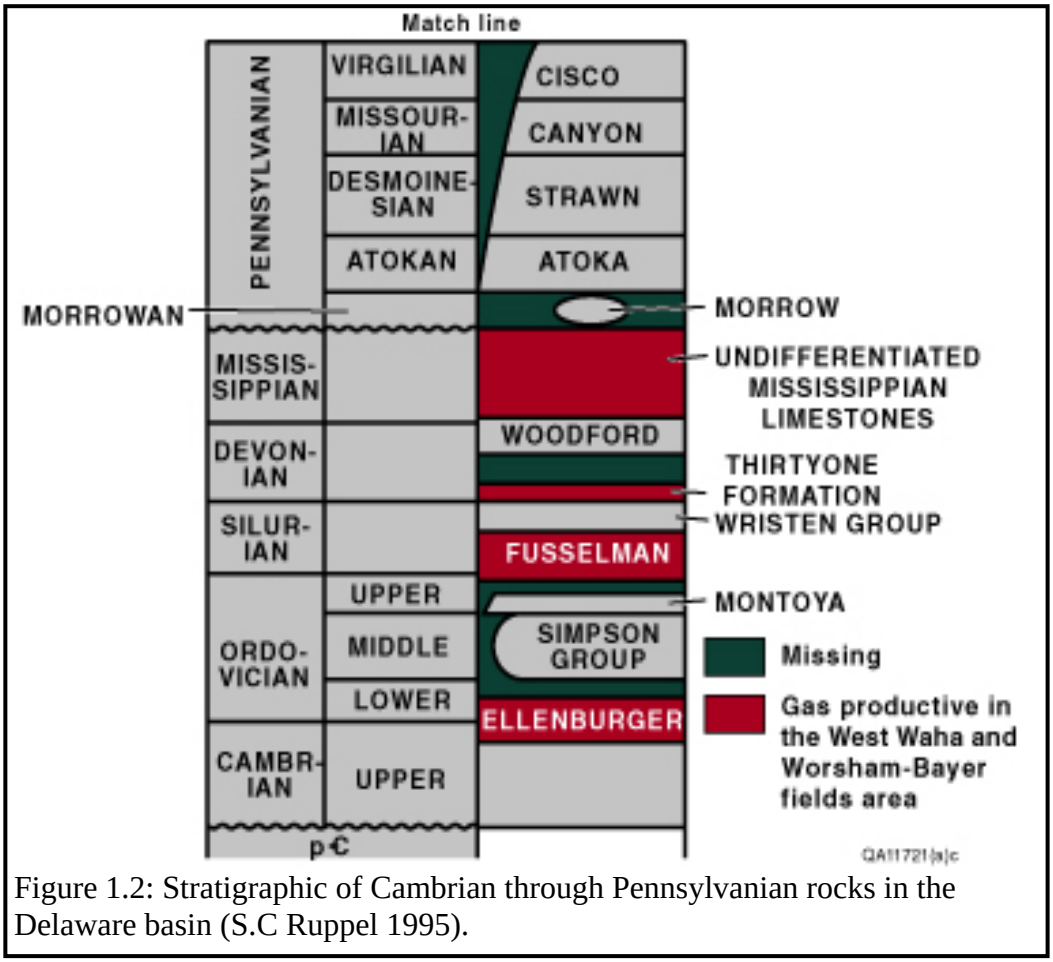

Figure 1.2: Stratigraphic of Cambrian through Pennsylvanian rocks in the Delaware basin (S.C Ruppel 1995).

1.1.1 Reservoir Geology of Ellenburger Group.

The Early Ordovician Group of western Texas consists mainly of dolomitized marine carbonate rock, with average thickness of 457 m around West Waha. The Middle Ordovician was marked by regional karsted weathering and erosion, forming the karstified part of the Ellenburger Group. (Kerans, 1990). The reservoir quality of the Ellenburger Formation is as a result of tectonic fracturing, brecciation, and karstification. Reservoirs of karstified Ellenburger Group low and varies from (2-7%) and moderate permeability that varies from (2-750mD).The Dolomitized Ellenburger has higher porosity of (2-14%) but its permeability is lower (1-44mD) than

karstified reservoirs (Loucks and Handford, 1992).

The Ellenburger Group of West Texas was divided based on reservoir quality into three units: (1) Karstified dolostone reservoir, (2) ramp carbonate, and (3) tectonically fractured dolostone based on reservoir quality (Holtz and Kerans, 1992). The karstified Ellenburger reservoir is located in the inner part of the platform where karstification plays an important role in the reservoir quality. This unit is located in the Central Basin Platform and Midland Basin of West Texas (Hardage and Hentz, 1998). The karstified Ellenburger has produced the largest amount of hydrocarbon in the Ellenburger Group, accounting for 37 percent of total production in the Ellenburger Group (Jones, 1953). The reservoir quality of the karstified Ellenburger unit is controlled by brecciation and karsting during the Middle Ordovician. Waters responsible for karstification were introduced through faults, fractures, and joints into the formation. Structural traps are faulted anticlines, and anticlines (Holtz and Kerans, 1992). Figure 1.3 shows the three major Ellenberger reservoir types in the study area.

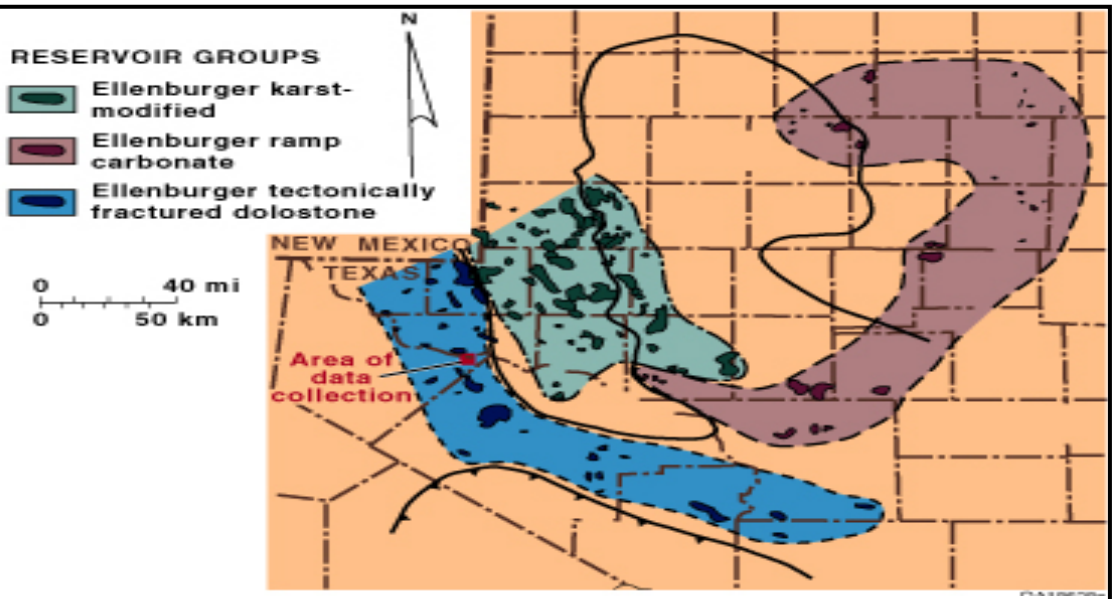

Figure 1.3: Three major Ellenberger reservoir types in West Texas.
(Holtz and Kerans, 1992).

The ramp carbonates Ellenburger unit is located in the southern Midland Basin and Eastern Shelf. It account for 4% of the oil and gas produced from the Ellenburger Group and contains 5% of the remaining oil and gas in place. The reservoir quality is as a result of the diagenesis history of the reservoir. Dolomitized packstone and limestone led to intercrystalline pore space and permeability (Holtz and Kerans, 1992). The structural controls of reservoir development are anticlines and faulted anticlines, while the seal is the overlying limestone (Ewing, T. E., 1991). These reservoirs are located in the Delaware and Val Verde Basins in West Texas. The porosity is 2-14 percent and with average permeability of 12mD (Levey et al. 1994).

The tectonically fractured Ellenburger reservoir forms the third unit within the Ellenberger Group in the West Waha and Worsham-Bayer fields. The reservoir quality resulted from tectonic fractures (Kupecz et al., 1991). This unit contains most

hydrocarbons accumulated in the Ellenberger Group. The fracture porosity and low permeability of this reservoir led to high gas mobility relative to oil, this being the reason for the production of no associated gas in the reservoir. The study area is adjacent to the Ouachita orogeny belt which resulted in complex structures within the area (Ewing, 1991).

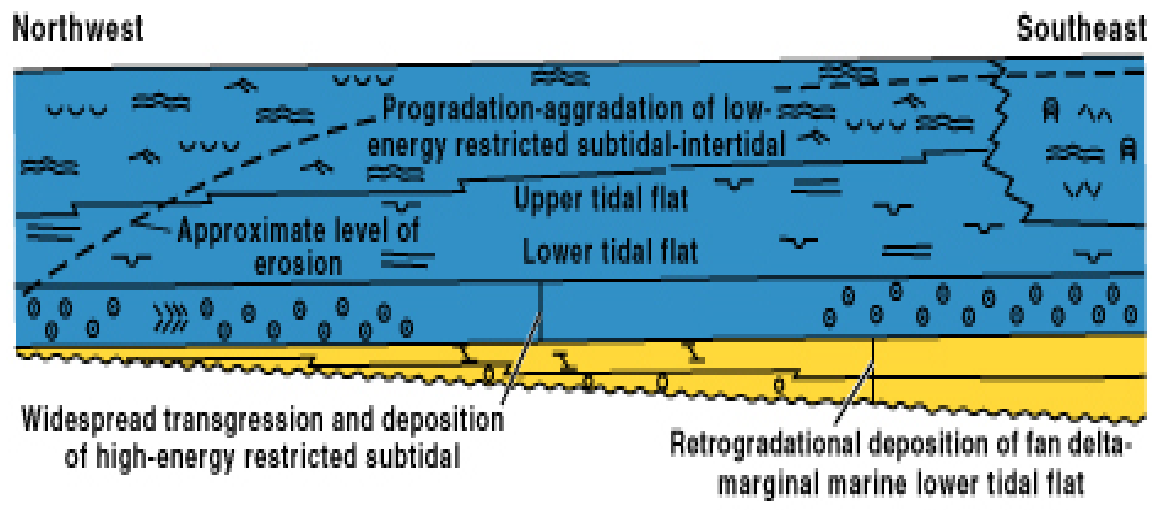

Figure 1.4: Schematic cross section of the Ellenberger facies assemblage over the crystalline basement (Hardage and Hentz, 1998).

1.1.2 Reservoir Geology of the Fusselman Formation

The Fusselman Formation is a member of the Silurian stratigraphic section in West Texas; it is composed of limestone and dolomites. It is overlain by the Silurian Wristen Group and underlain by the Ordovician Montoya Group (Ruppel and Holtz, 1994). The northern West Texas part of Fusselman is dolomitize and they are limestone in the region of West Waha and Worsham-Bayer fields. The Fusselman was described as a shallow-water carbonate facies containing porous and permeable basal ooids overlain by fenestral mudstones and underlain by thick pelmatozoan grainstone and packstone containing spar

and voids interpreted has leaching events (Ruppel and Holtz, 1994). The Fusselman reservoirs have been categories in the Shallow-Platform Carbonate play and have produced oil from over 300 reservoirs in West Texas (Holtz et al., 1997).

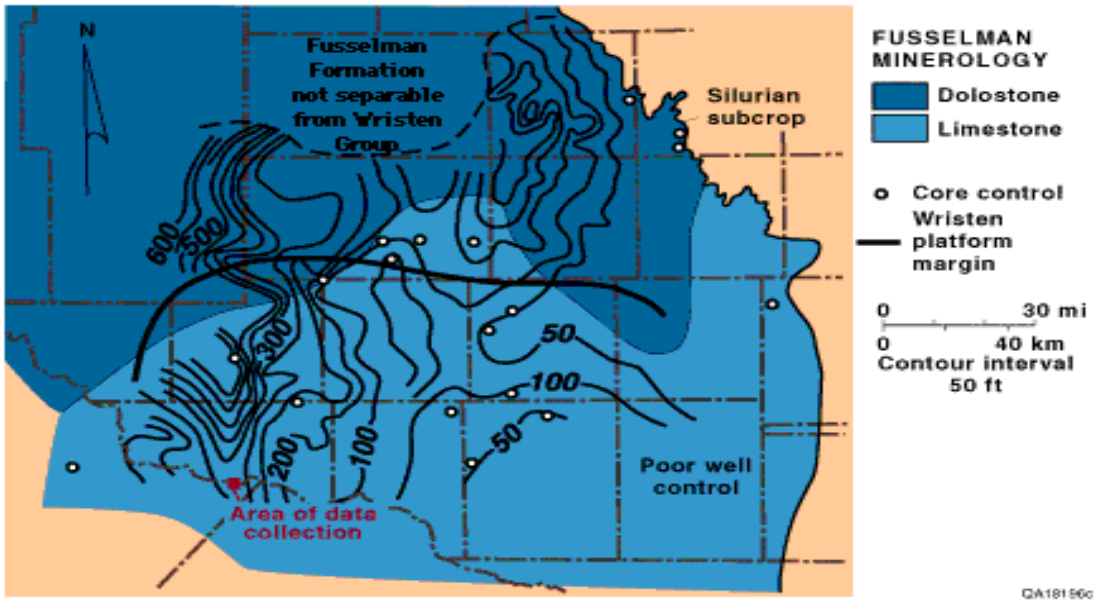

Figure 1.5: The distribution of the dolostone and limestone of the Fusselman group (Ruppel and Holtz, 1994).

1.1.3 Reservoir Geology of Thirtyone Formation.

The Thirtyone Formation belongs to the Devonian stratigraphic section around the West Texas and Worsham Bayer fields. It is underlain by the Wristen Group and overlain by the Woodford Formation (shale) which serves as the source rocks to the reservoirs in the Delaware Basin (Jones, T.S., 1953). The Thirtyone Formation is a hydrocarbon reservoir of limestones, dolomites and cherts. The reservoir quality is controlled by vuggy, intercrystalline, and fracture porosity. The deposition history, as described by Ruppel and Holtz (1994), has basin siliceous sediments due to transgression by prograding and aggrading carbonate sediments into a shallow water ramp. As shown in figure 1.6. The

cherts were deposited as a result of pelagic sedimentation and turbidite flow in the down slope direction. The composition of the Thirtyone Formation is more siliceous towards the base and relatively carbonate upward. Ruppel and Holtz (1994), classified the formation into the following facies: dark color chert/carbonate laminite, thick bedded laminate chert, burrowed chert, and skeletal packstone. The Thirtyone Formation is divided into two oil productive plays which are the ramp carbonate play and the deep water chert play. The Thirtyone Formation in the West Waha and Worsham-Bayer fields is predominantly a gas reservoir. The reservoir quality is controlled by conversion of silica phases from metastable to stable silica during deposition and compaction (Ewing, 1991).

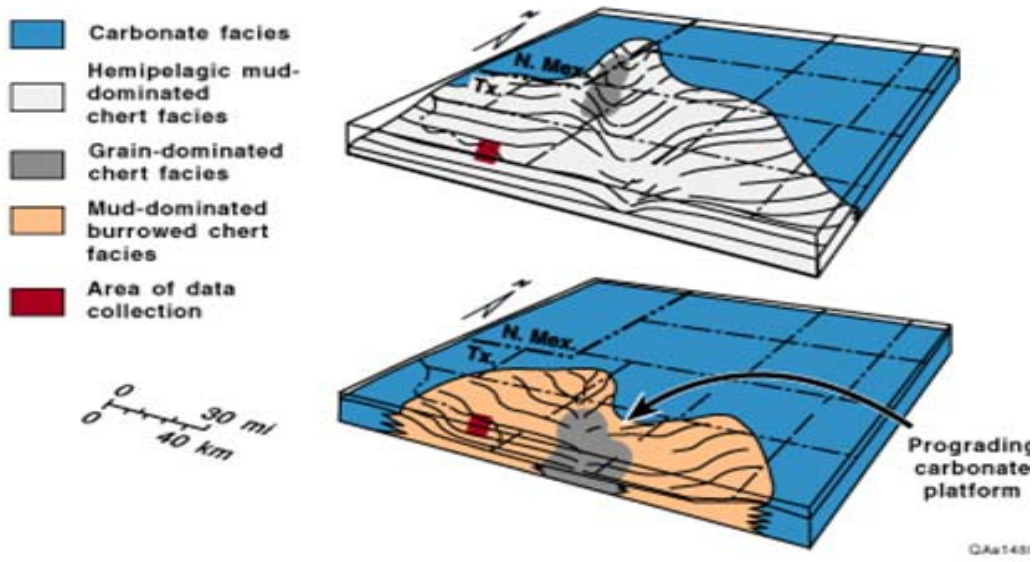

Figure 1.6: Facies distribution of Thirtyone Formation during deposition in West Texas (Ruppel and Holtz, 1994).

1.2 Data Set

The field data are owned by Gas Research Institute (GRI) and US Department of Energy (DOE). The data set consist of 3D time migrated stacked sections, 11 well logs and production data of the West Waha Worsham Bayer Fields, Delaware Basin, West Texas. Figure 1.7 shows the location of the wells within the seismic section.

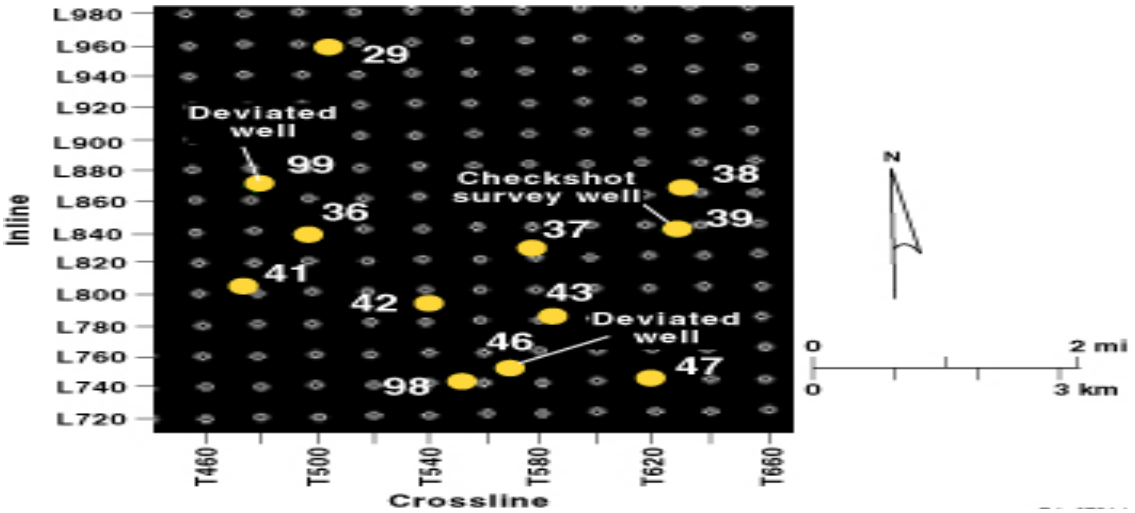

Figure 1.7: Location of the wells within the seismic section (Hardage and Hentz, 1998).

1.2.1 Borehole Data

The borehole data consist of 11 well logs, a checkshot survey, and directional wells. All well logs include gamma ray, sonic, neutron, or density logs, and electrical (resistivity or induction), caliper, and SP logs. Figure 1.8 is a well log of the study area containing sonic and gamma ray logs.

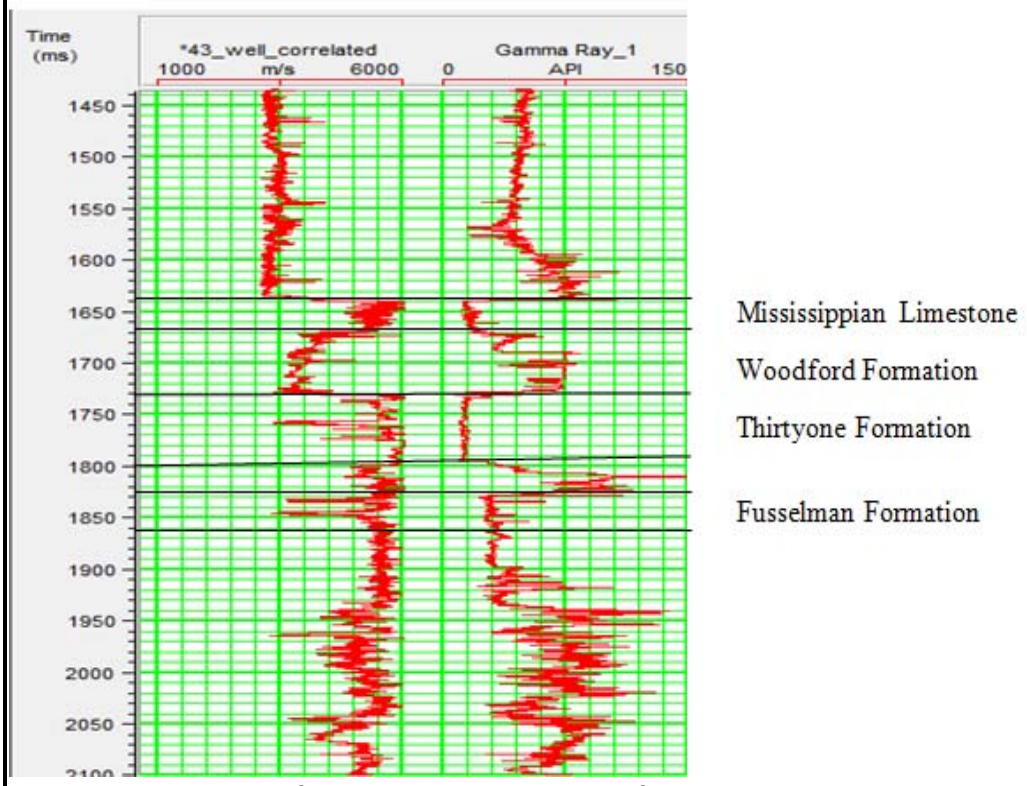

Figure 1.8: Well log of the study area with identified reservoirs

1.2.2 3D Seismic Data

The seismic data is approximately 51.8 km^2. Three-Dimensional post stacked migrated data set. It has 261 inlines (720-980) and 201 crosslines (460-660), sampling rate of 4ms and the time range is 0 – 4s with average amplitude of 3.61. The stacking bins are 33.5 m. The line number byte position is 9 to 12 and the trace number byte position is 21 to 24. The seismic section is shown in 3D view in figure 1.9 with time slice at 2s.

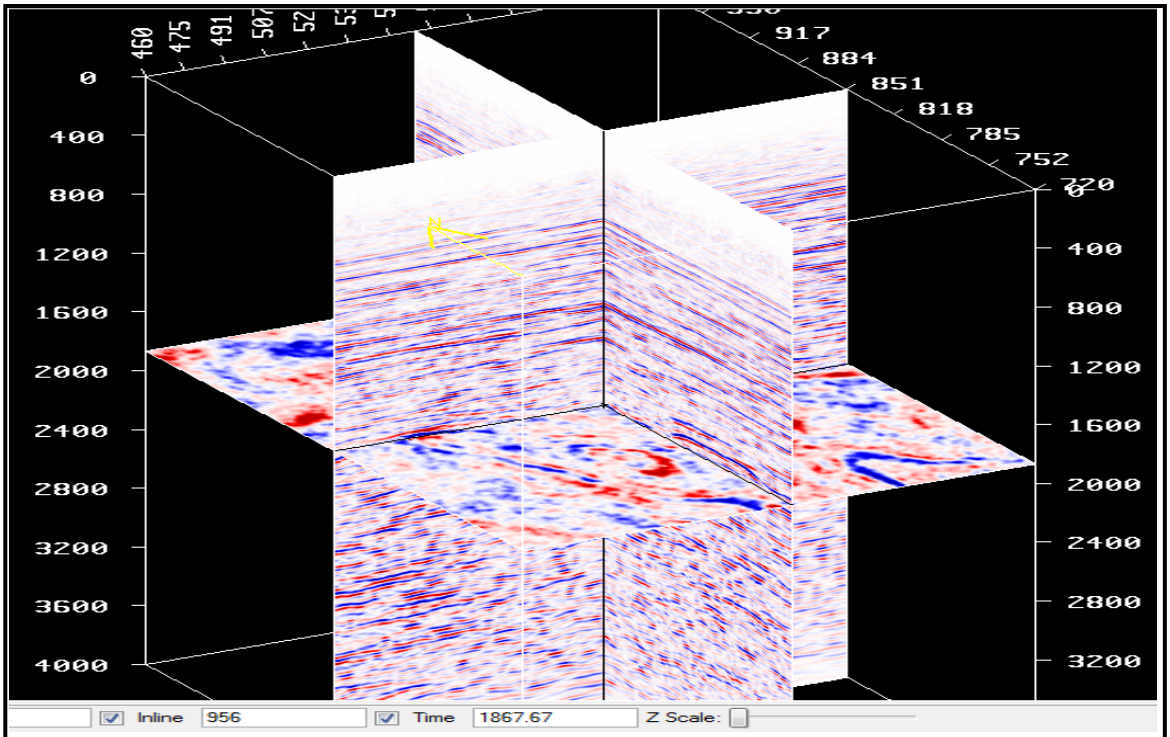

Figure 1.9: 3D view of the seismic section and a time slice at 2s.

1.3 Research Workflow

1.3.1 Well Log Preparation

The well logs were quality checked to note if logs for lithology and fluid identification are in place for each well, where they are not, density logs were generated by inversion using the Gardener's equation and carefully estimating P-wave velocity from sonic logs. Also, pseudo sonic logs were generated using the Han's transform. These steps are necessary because density and sonic logs are used to compute impedance log and reflection coefficient, which are convolved with wavelet to generate synthetic seismogram.

1.3.2 3D Seismic Analysis

The 3D seismic data were quality checked by eye to catch reflections with traps, closures, and structures such as bright spot, flat spot, faults, etc. The seismic and well logs are then correlated, and time to depth conversion was done. This was followed by identifying lithology/reflections of interest on the vertical seismic section and horizons of interest were picked. The seismic section was then cropped into sub cubes of interest to speedup computation rate of spectral decomposition and to minimize extraneous data that have no significance to the study.

1.3.3 Attribute Analysis

This process involves generating attribute maps for the picked horizons to emphasize features of interest. These features of interest may include localized amplitude anomalies associated with variation in geology.

1.3.4 Spectral Decomposition and Interpretation

This involves decomposing the broadband seismic into its constituent frequencies. It is a time frequency transformation that transforms time domain seismic data into the frequency domain. The techniques used in this transformation include: Continuous Wavelet Transform (CWT), Discrete Fourier Transform (DFT), and Constrained Least Squares Spectral Analysis (CLSSA). Using these techniques, frequency volumes that correspond with discrete energy in the seismic band were generated with the same sampling rate as the original broadband seismic. A total of one hundred and twenty-five (125) frequency volumes corresponding to the frequency bandwidth of the original

seismic data were generated. This was followed by analyzing each frequency volume for amplitude anomalies that are associated with the gas-bearing formations.

The amplitude spectrum from these various techniques were computed for a single seismic trace, and then for a seismic horizon and the results compared with one another to access effectiveness of each technique. Figure 1.10 shows the workflow of the research work.

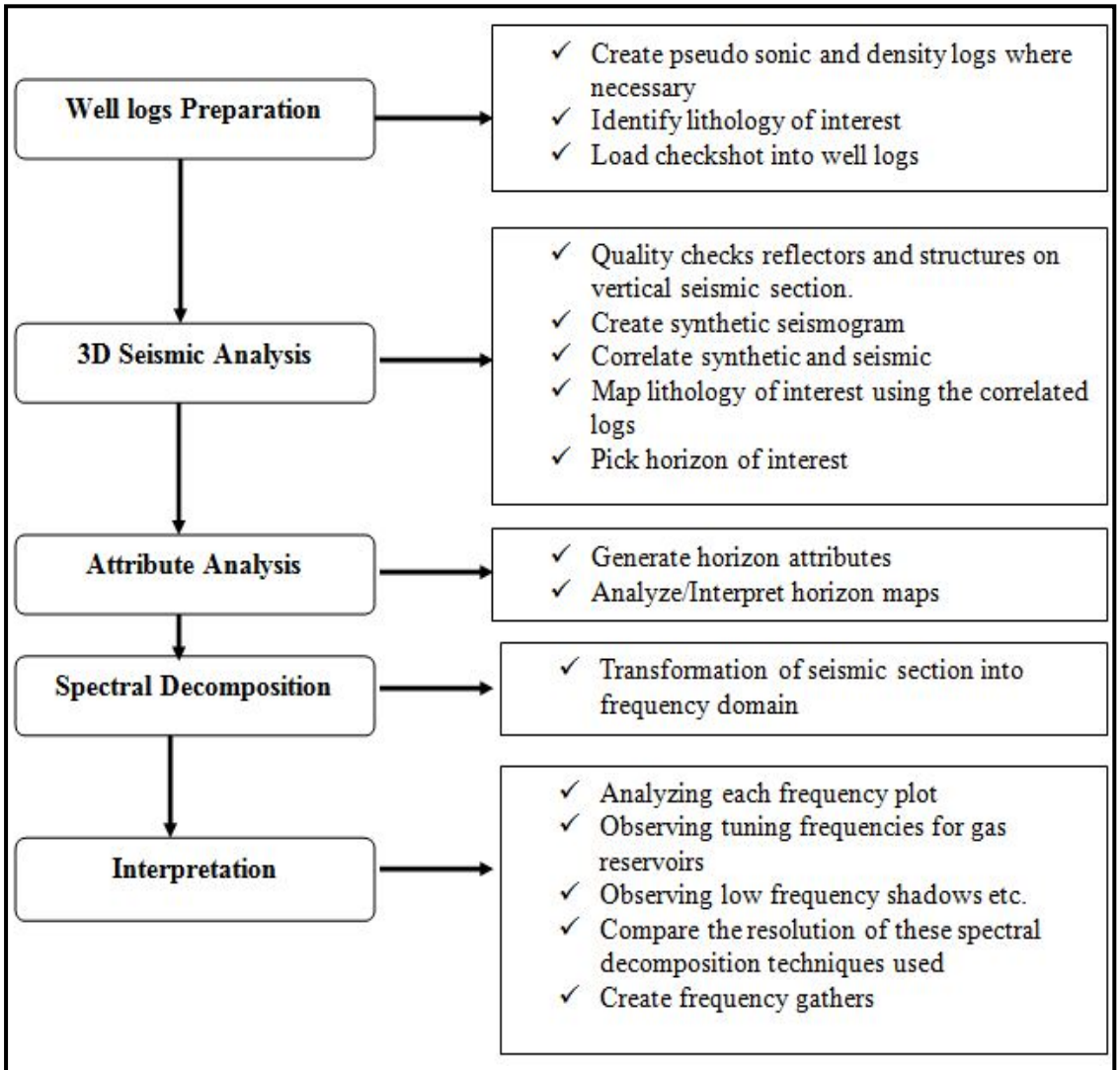

Figure 1.10: Shows the workflow of the research work.

Chapter Two

2.0 Data Interpretation

2.1 Well Log Interpretation

Well log interpretation is important to properly analyze the diagnostic features of rocks and fluid properties in the reservoir. Several well log data were available for the study area, but only two wells (Well 37 and Well 46) were utilized in this research (figure 2.1). Both wells were supplied with a suite of log data that include: gamma ray, resistivity, density, and sonic logs. The logs are displayed below in figure 2.1 with the reservoirs identified and correlated on both well logs.

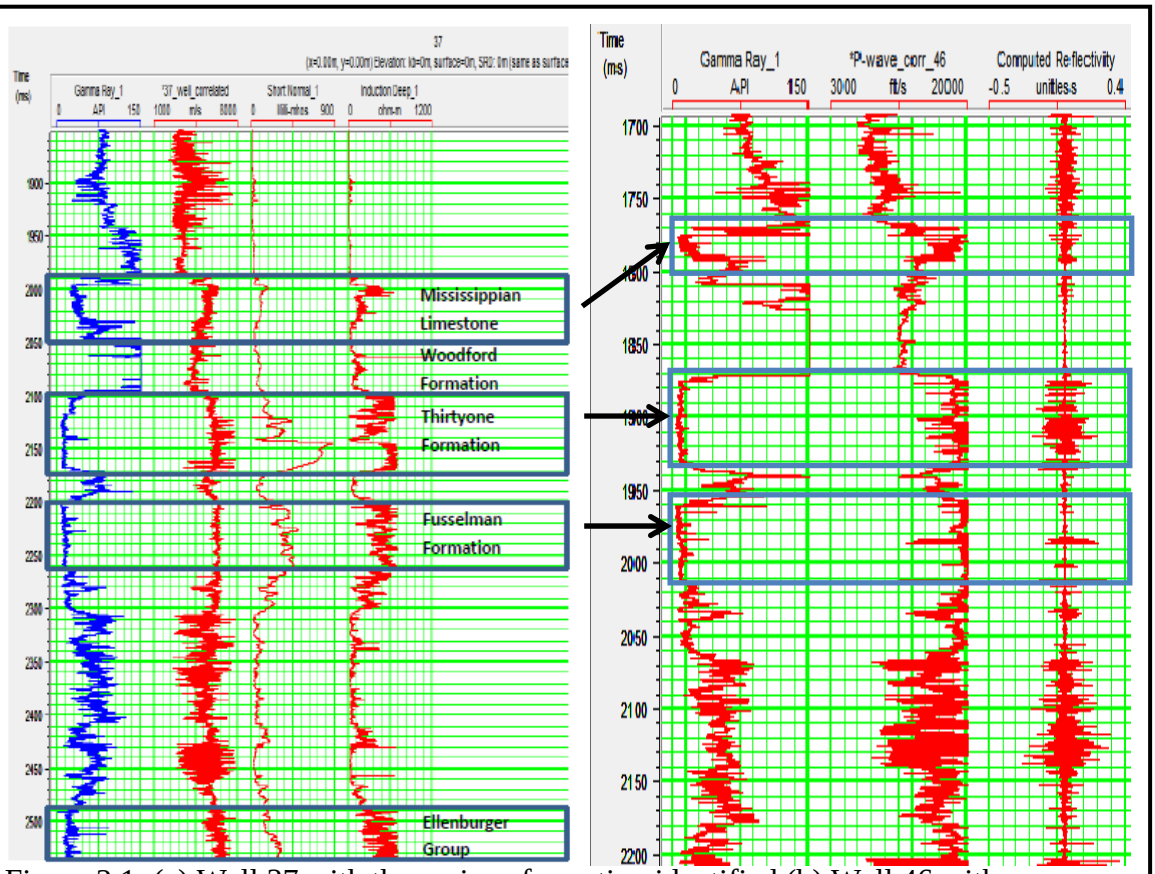

Figure 2.1: (a) Well 37 with the various formation identified (b) Well 46 with the corresponding lithology identified.

2.2 Gamma Ray Log

Gamma ray logs measure the radioactive content of formation. Shale formations have high radioactive content, explaining the high gamma ray reading observed in shales. Shale-free formations such as sandstones and carbonates have low radioactive contents, and thus have low gamma ray readings. Exceptions to this are sandstones containing potassium feldspars, micas, and glauconite (Asquith, 1982).

The study area is a carbonate environment without feldspars and micas. The Woodford shale unit has high gamma ray reading as seen on Well 37 (figure 2.1a) around 2050 ms - 2100 ms, representing the source rock in this field. The same formation (Woodford Formation) is seen on Well 46 (figure 2.1b) with high gamma ray reading at 1800 ms – 1870 ms. The Mississippian limestone (gas reservoir) on Well 37 is shown to have a low gamma ray reading at 2000 ms -2050 ms. This corresponds to the low gamma ray reading at 1760 ms – 1810 ms on Well 46. The limestone and dolomitic Thirtyone Formation is indicated by low gamma ray reading at 2100 ms – 2170 ms on Well 37, which corresponds to low gamma ray reading on Well 46 at 1870 ms -1940 ms. The Fusselman Formation and Ellenburger Group are also represented by low gamma reading on Well 37 and Well 46 as shown in figure 2.1.

2.3 Sonic Log

The sonic log measures the interval transit time (Δt in $\mu s / ft$) of a compressional sound wave travelling through one foot of formation. The transit time is dependent upon both lithology and porosity (Asquith, 1982). Well 37 shows the Mississippian limestone with compressional wave velocity of 4900 m/s and Well 46 shows that the Mississippian

limestone has a velocity of 5400 m/s. The underlying Woodford shale has a velocity of 3500 m/s on Well 46 and Well 37. The Thirtyone Formation (dolomite and limestone) has a velocity of 5500 m/s on Well 37 and velocity of approximately 6000 m/s on Well 46 typical of limestone reservoirs.

2.4 Resistivity Log

Resistivity is an electrical property of materials that describes the ability to resist the flow of electric current. It is the inverse of conductivity. Brine-saturated rocks are conductive and have low resistivity because they contain free ions that support the flow of current. The short normal and the induction logs are the electrical type logs available for this research on Well 37 (figure 2.1a). All the reservoirs have high resistivity values when compared with the Woodford shale with low resistivity of approximately 150 ohm/m on the deep induction log. The Mississippian limestone has an average of 240 ohm/m on the deep induction log. Thirtyone Formation has about 720 ohm/m and the Fusselman Formation has 480 ohm/m-720 ohm/m as compared with the overlying shale formation with less than 100 ohm/m. The high resistivity values in the reservoirs indicate the presence of hydrocarbon.

2.5 Seismic to Well Correlation

Seismic to well correlation is the measure of similarity between pair of traces (Asquith, 1982). This process involves generating synthetic seismogram from the drift corrected sonic and density logs and comparing it with a composite seismic traces extracted around the well location on the seismic section. Drift correction is applied to the sonic log to shift the seismic to a reference datum and also to correct for dispersion effects arising

from high frequency contents of sonic logs. Drift correction is important because of the following reasons:

1. The first layer velocity is often unknown.
2. Seismic data may have time stretch due to frequency dependent absorption and short period multiples (Asquith, 1992).
3. There are greater dispersion and absorption on surface seismic as compared to sonic log.

Creating Synthetic Seismogram

Generating synthetic seismogram is an important aspect of correlation. The following steps are essential in generating synthetic seismogram:

1. Drift correction on sonic log.
2. Calculate acoustic impedance $(Z): Z = \ell v$ from the density and sonic logs.
3. Calculate reflection coefficient (R) between successive pair of acoustic impedance to generate a reflectivity series.

   $$R = \frac{Z_2 - Z_1}{Z_2 + Z_2}$$

4. Convolve the reflectivity series with the desired wavelet $(S(t) = W(t) * r(t))$

   Where $S(t)$ is the seismogram, $W(t)$ is the wavelet, * is the convolution operator and $r(t)$ is the reflectivity series.

This research involves generating synthetic seismogram by convolving the reflectivity series with wavelet extracted from the wells and seismic for correlation as shown in figures 2.3. The well to seismic correlation coefficient for this well is 0.69 shown in red

circle. The Mississippian Formation location is highlighted with the black circle and the Fusselman Formation is in yellow circle. The wavelet extracted from the Well 37 and Well 46 are shown in figure 2.2.

a) Well 37 Wavelet

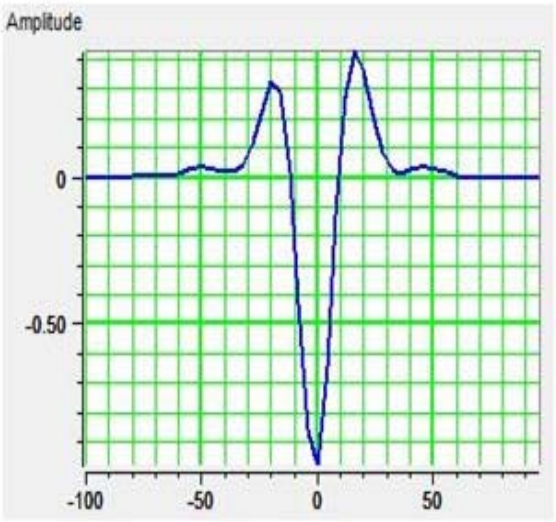

b) Well 46 Wavelet

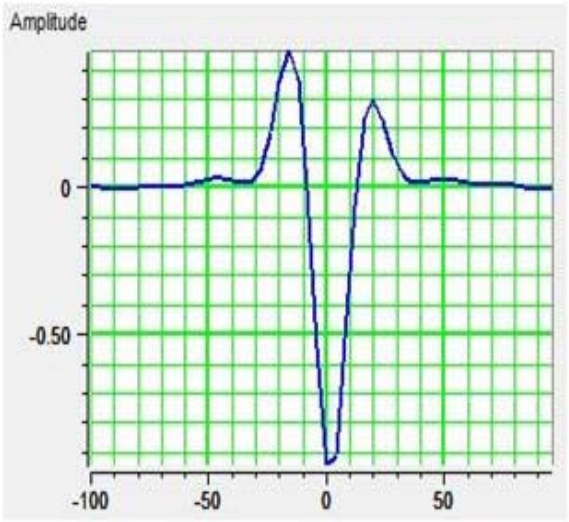

c) Well 37 Frequency Spectrum

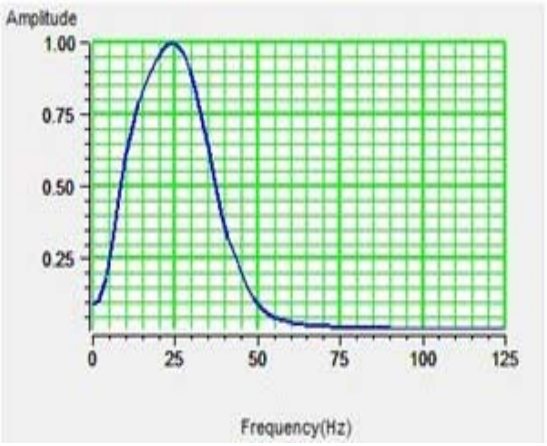

d) Well 46 Frequency Spectrum

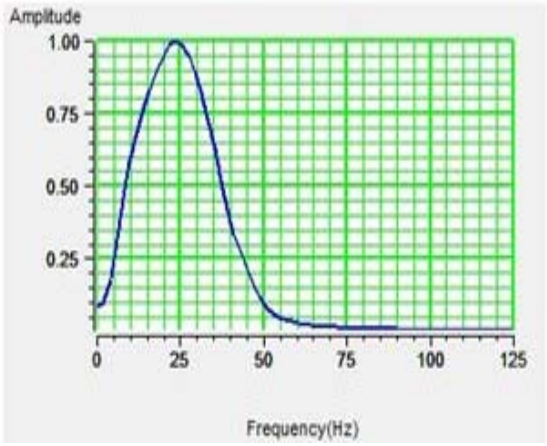

Figure 2.2: (a) Wavelet extracted from the seismic at Well 37 location (b) Wavelet extracted fromWell 46(c) Frequency spectrum of the wavelet extracted from Well 37 (d) Frequency spectrum of wavelet extracted from Well 46.

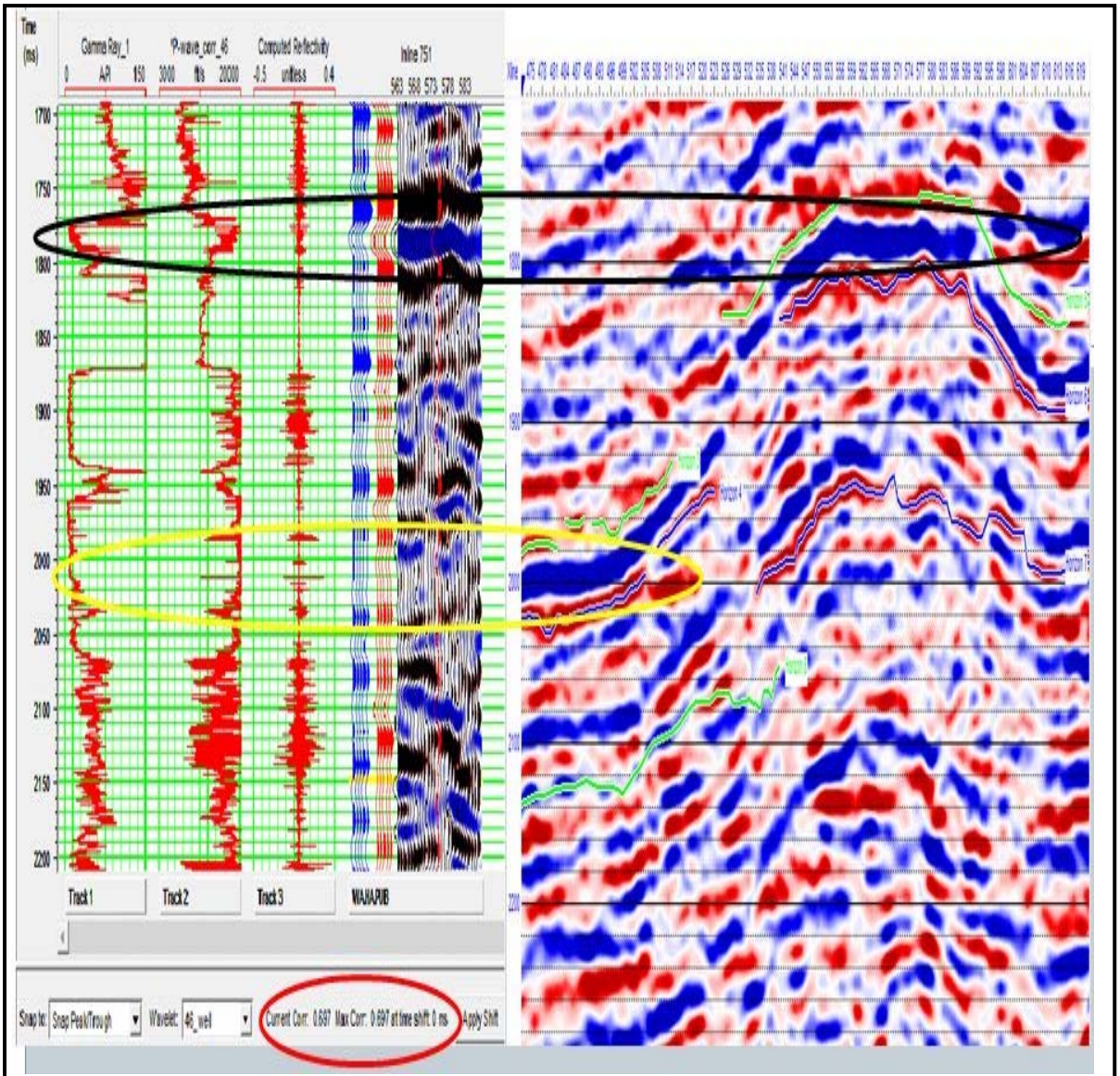

Figure 2.3: Correlation panel of well 46 with seismic. The black circle is the position of the Mississippian Limestone and yellow circle is the position of the Thirtyone formation

2.6 Horizon Interpretation

Gao (2007) described horizon interpretation as “an interpretational concept that separates different geological units such as: water from shallow sediments, sedimentary rock from salt diapirs or Tertiary clastic from Mesozoic carbonates”. This research is focused on picking horizons at the top of the reservoir and through the low frequency shadow at low and high

frequencies to analyze the changes in amplitude at each frequency. Horizon slices through the 25Hz and 65Hz DFT volumes corresponding to the top of the reservoir and the low frequency shadow are shown in figure 2.4.

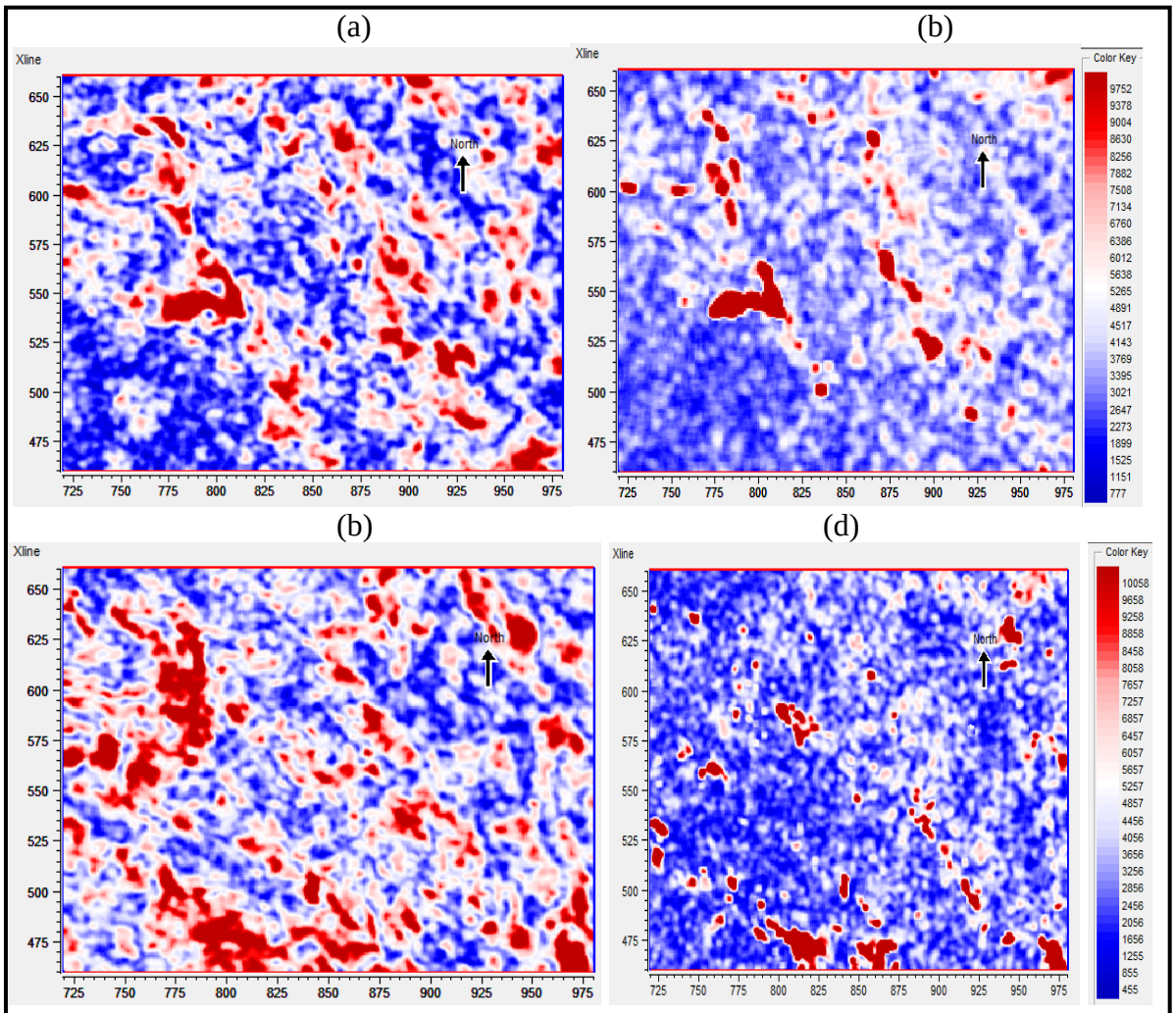

Figure 2.4(a) Amplitude extraction on DFT 25Hz at 20ms above the reservoir.
(b) Amplitude extraction on DFT 25Hz through the low frequency shadow.
(c) Amplitude extraction on DFT 65Hz at 20ms above the reservoir. (d) Amplitude map of DFT 65 through the low frequency shadow.

Also, horizon picks along a channel were done to investigate the power of the techniques for structures delineation. Figure 2.5 show the seismic section with black arrow pointing to the

channel and picked horizon is indicated by yellow line. The Root Mean Square (RMS) amplitude of the horizon is shown in figure 2.6 with the black arrows pointing to the channel.

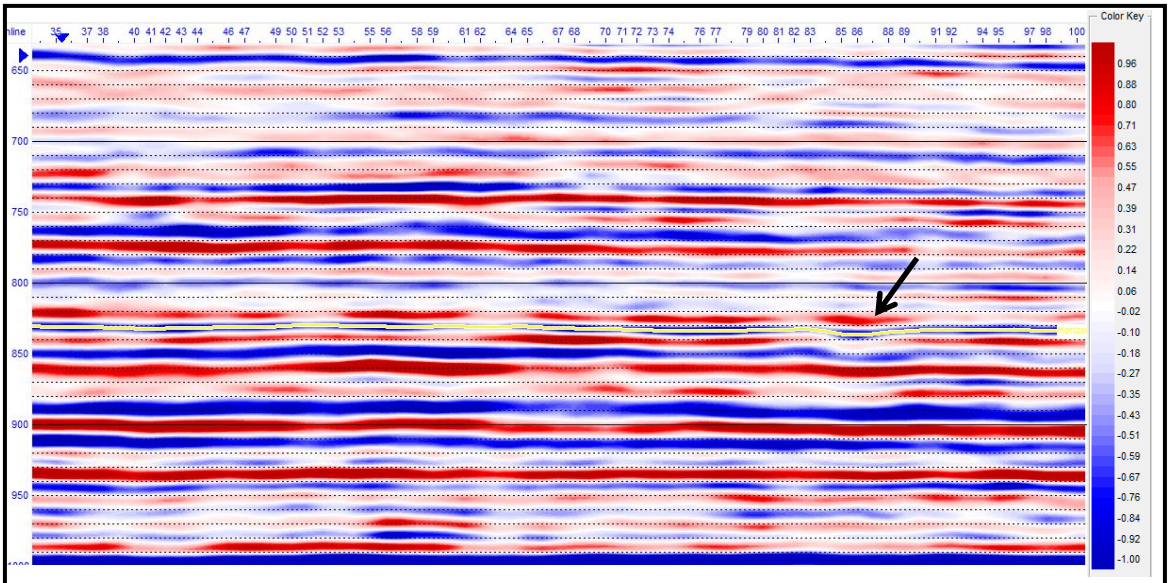

Figure 2.5: Seismic section showing the picked horizon (yellow) and the black arrow pointing at the channel.

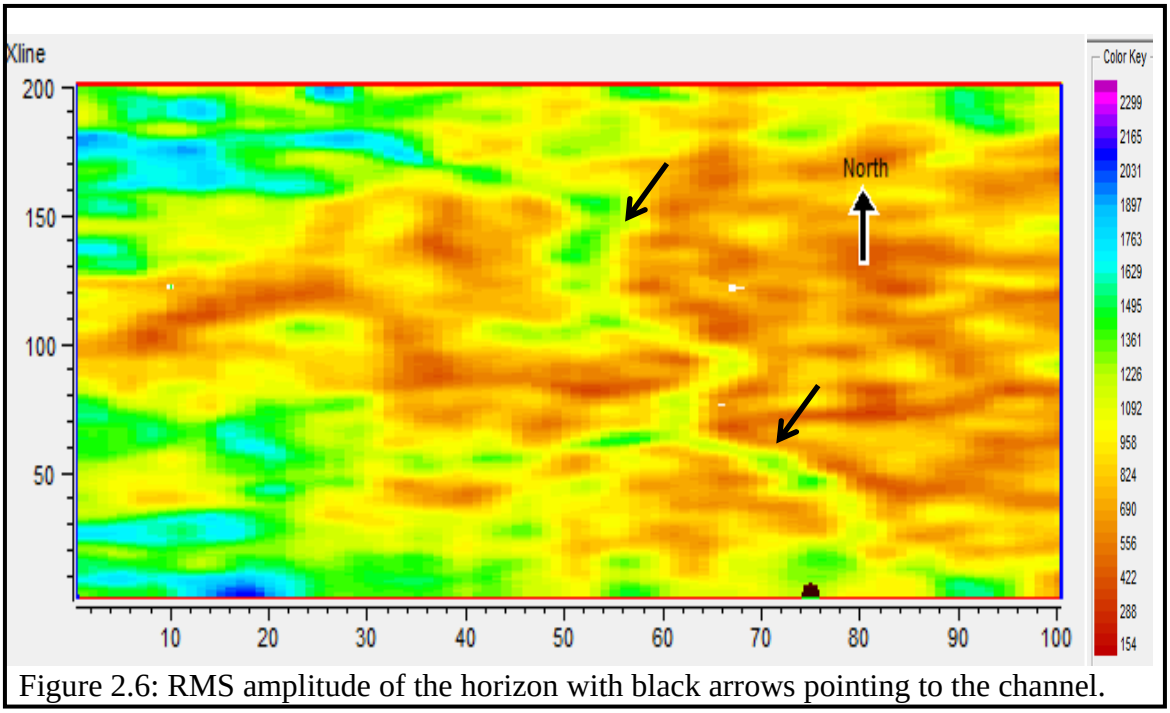

Figure 2.6: RMS amplitude of the horizon with black arrows pointing to the channel.

Chapter 3

3.0 Methodology

3.1 Spectral Decomposition

Partyka et al. (1997) introduced the concept of spectral decomposition as a post-processing method for quantifying and visualizing subtle seismic tuning effects. It is defined as a seismic analysis technique that decomposes seismic data into time-frequency domain which makes it possible to extract useful information such as layer thickness (Partyka et al., 1999), direct hydrocarbon detection (Castagna et al., 2003, Wei et al., 2011), or stratigraphic interpretation (Marfurt et al., 2001). This is possible because subtle features not visible on time domain seismic data can be emphasized on frequency domain sections. Localization of events such as reflections, noise, and surface waves are also possible in the frequency domain, thus making separation and elimination of undesired events possible (Okaya et al., 1995).

The Short Time Window Fourier Transform (STFT) of spectral decomposition, unlike traditional Fourier Transform, assumes variable statistic for the seismic signal which allows the extraction of frequency content unique to all the time samples. The geology of the signal becomes less random. Analyzing the amplitude and phase spectra of the frequency volume expresses the temporal frequency distribution of the signal (Partyka et al., 1999). This is because a reflectivity series, when convolved with a source wavelet in the presence of noise for a long analyzing window approximate the wavelet spectrum (figure 3.1). That is, it sums up the effects of the individual thin beds within the window, flattening the amplitude spectrum (Partyka et al., 1997). A short window does

not approximate the effect of the thin beds and its response is determined by the acoustic properties, thickness of the layers within the window, and the geology. Hence the resulting amplitude spectrum represents the interference pattern of the window as shown in figure 3.2.

Spectral decomposition is useful in delineating subtle features and thin beds because thin bed reflectivity has a characteristic response in the frequency domain (Castagna et al., 2003). The output of spectral decomposition is a series of amplitude and phase spectra tuned to specific frequencies. The amplitude spectrum is essential in estimating bed thickness in time domain while the phase spectrum is used to define geologic/stratigraphic discontinuities (Partyka et al., 1999). Time-frequency analysis of a seismogram can be achieved in many ways, some of the methods include: The Fourier-based methods (Short Time Fourier Transform, Fast Fourier Transform), the wavelet-based methods (Continuous Wavelet Transform and Discrete Wavelet Transform) and those that depend on wavelet dictionary selection (Matching Pursuit Decomposition). The STFT is a Fourier-based method for time-frequency analysis of a seismogram. It transforms a 1D signal in time into a 2D time-frequency representation by taking a continuous fixed short time window along the time axis (Okaya et al., 1995).

Mathematically, it can be represented as:

$$F(\tau, w) = \int_{-\infty}^{\infty} f(t) g(t-\tau) \ell^{-jwt} dt \qquad (1)$$

where $g(t)$ is the window function, $f(t)$ is the seismogram to be transformed, ℓ^{-jwt} is the Fourier kernel

STFT can also be performed on frequency domain by sampling along the frequency axis with fixed bandwidth band-pass filter (Okaya et al. 1995). The major pit fall of the STFT is the fixed resolution problem due to the fixed predetermined analyzing window length. A wide window gives better frequency resolution and poor time resolution and a short window gives good time resolution and poor frequency resolution (Castagna et al., 2003). When the window length is too short, smearing of energy across bandwidth is observed on the STFT spectrum beyond the band of the original seismic data. If the window length is too long, interference is observed between non isolated reflections within the window, degrading the time resolution (Castagna et al., 2003). The wavelet analysis method was introduced to improve the resolution problem of the STFT. Continuous Wavelet Transform and Discrete Wavelet Transform are based on the superposition principle that states that the frequency spectrum of a seismogram is the sum of the constituent frequency spectra of the wavelet that sum up to produce the seismogram (Castagna et al., 2003). CWT scales and translates the basis wavelet by applying bandpass filter to produce series of wavelets, which are convolved with the seismogram to yield time-frequency panels. Discrete Wavelet Transform (DWT) decomposes a function by applying a band-pass filter to the original signal at different bandwidths, unlike CWT, the DWT uses quadrature mirror filters to decompose a seismogram. Both CWT and DWT have resolution limitations at intermediate frequencies. Matching Pursuit Decomposition (MPD) is another time-frequency analysis method that has good intermediate to high frequency resolution. This method of signal decomposition requires selection of wavelet from a suite of wavelet dictionary. It scales, translates, and modulates a single window

function to produce a set of basis functions (Okaya et al., 1995). MPD introduces artifacts into the time-frequency analysis over wide frequency band or long time interval (Castagna et al., 2003).

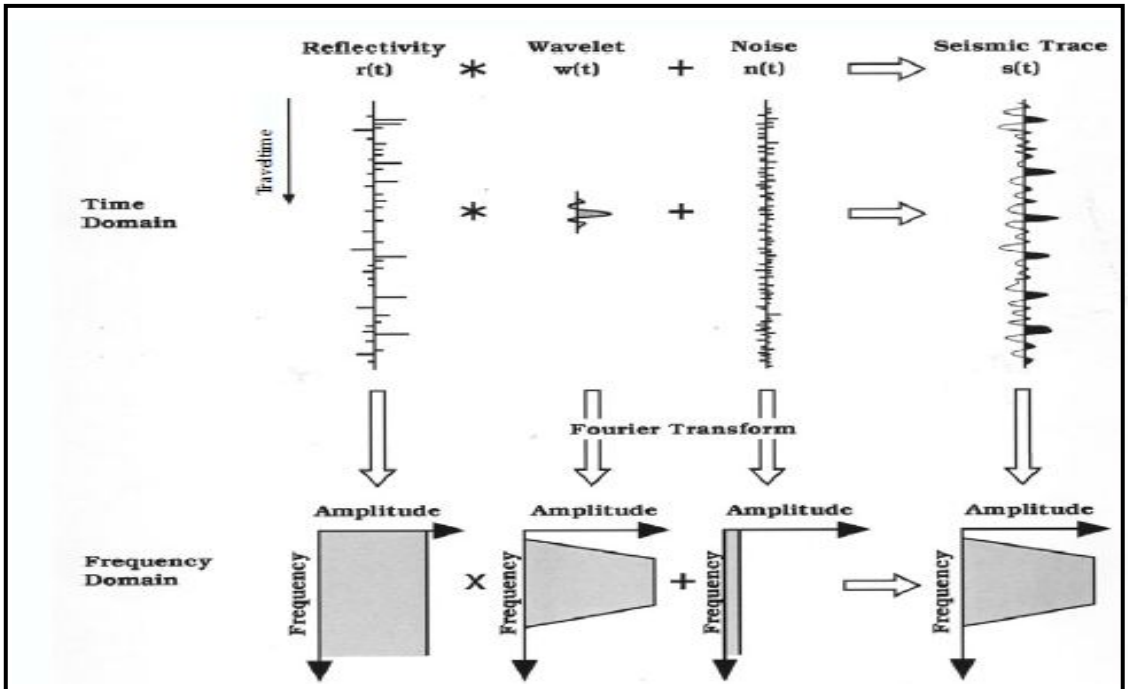

Figure 3.1: Convolution model of a long window spectral decomposition. (Partyka et al.,1999).

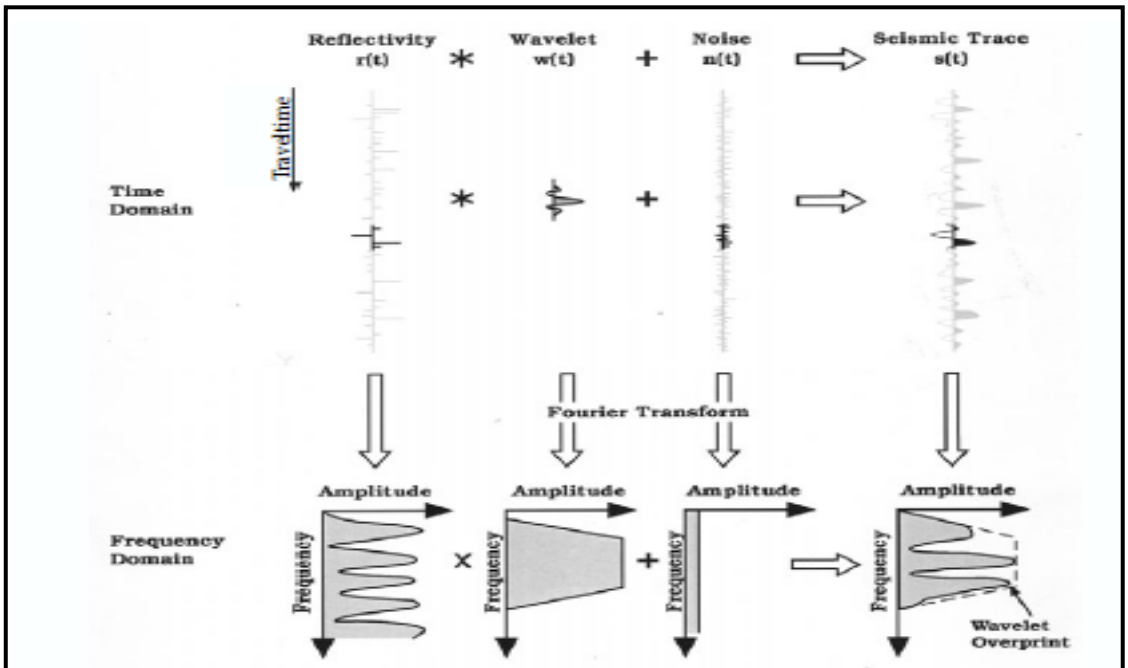

Figure 3.2: Convolution model of a short window spectral decomposition (Partyka et al., 1999).

3.2 Spectral Decomposition as Hydrocarbon Indicator

Castagna et al. (2003) described the use of spectral decomposition as hydrocarbon detection technique. They analyzed the frequency response of amplitude variation caused by variation in fluid properties, thickness, and porosity. The frequency response also aids in the interpretation of the reservoir geomorphology and structural complexity. Castagna et al. (2003) identified three unique spectral responses associated with hydrocarbon bearing zones. These responses are:

(i) Abnormal seismic attenuation in thick reservoirs.

(ii) Low frequency shadows beneath the reservoir.

(iii) Differences between tuning frequency of gas sands and brine sands.

3.3 Low Frequency Shadow

The concept of low frequency shadow beneath gas charged reservoirs is an old and familiar concept,(e.g Taner and Sheriff, 1979, Castagna et al., 2003), but the cause of this phenomenon is not clearly understood. Different authors have attempted to explain the precise cause of the low frequency shadow beneath gas reservoirs. In a reservoir with energy absorbing fluid and sufficient thickness, it might be reasonable to conclude that the low frequency shadows beneath the reservoirs are due to attenuation. But in thin reservoirs where there is no enough travel paths for the seismic waves, one cannot conclude that low frequency beneath the reservoir is due to seismic energy attenuation (Castagna et al., 2009).

Dan Ebrom (2006) described the likely causes of low frequency shadow. He classified these causes into two categories which are, stack-related effects and non-stack -related

effects. Stack- related effects reduce the apparent frequency by selectively suppressing higher frequencies. Non-stack related effects could be due to intrinsic attenuation, multiple reflections from the top and bottom of a gas reservoir. Attenuation is like a low pass filter, it suppresses higher frequencies more than lower frequencies. Some reservoirs usually have a low attenuation coefficient (Q factor) than its background and exhibit zones of anomalous absorption lying in a larger background region (Winkler and Nur, 1982).

Wang, 2007 investigated the effects of attenuation on a seismic section, he applied an inverse Q filter to compensate high frequency energy loss due to attenuation and phase distortion resulting from frequency dispersion (figure 3.3). After running spectral decomposition on both data set (original seismic and the inverse Q filtered data), the spectral decomposition shows that low frequency shadows still exist on the inverse Q filtered data which implies that low frequency shadows beneath gas reservoirs are not entirely due to attenuation. Castagna et al, (2009), investigated the cause of low frequency shadows in reservoirs by building wave equation based synthetic wedge model in which the wedge has a velocity and density close to that of gas sand and it is embedded in between high impedance rock with velocity and density similar to shale. They compared the frequency response due to attenuation, differences in velocity of brine sand and gas sand, and thickness. They conclude that the low frequency shadows are as a result of the low velocity of gas filled reservoir which causes time sag below the reservoir. Figure 3.5 shows spectra shifts due to gas accumulation in the reservoir.

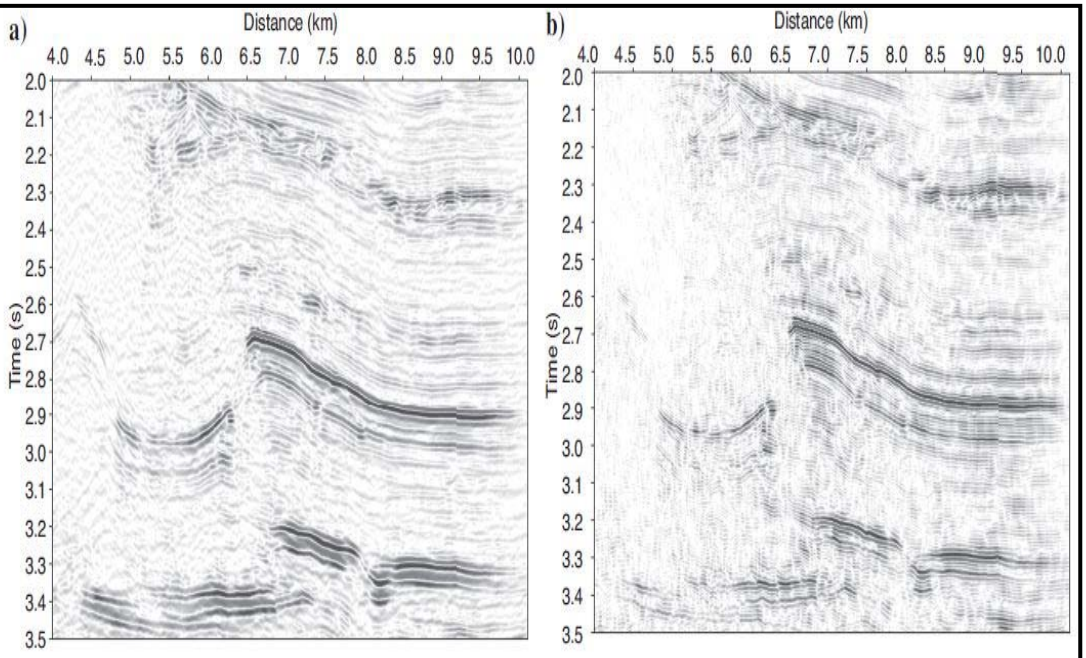

Figure 3.3: (a) The seismic section without inverse-Q filtering and, (b) the section after inverse Q filtering. The filtered section shows reflections wavelets that are narrow from shallow to deep. (Wang, 2007).

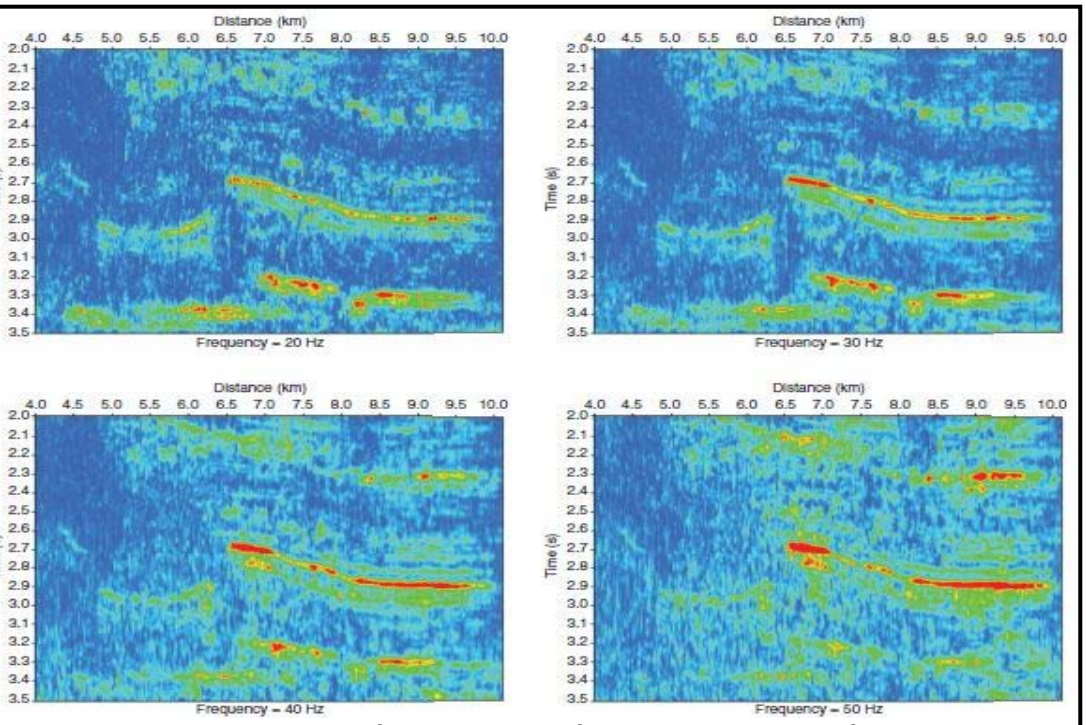

Figure 3.4: Frequency cubes of the inverse-Q filtered section. Low frequency shadows still exist on the cubes. (Wang, 2007).

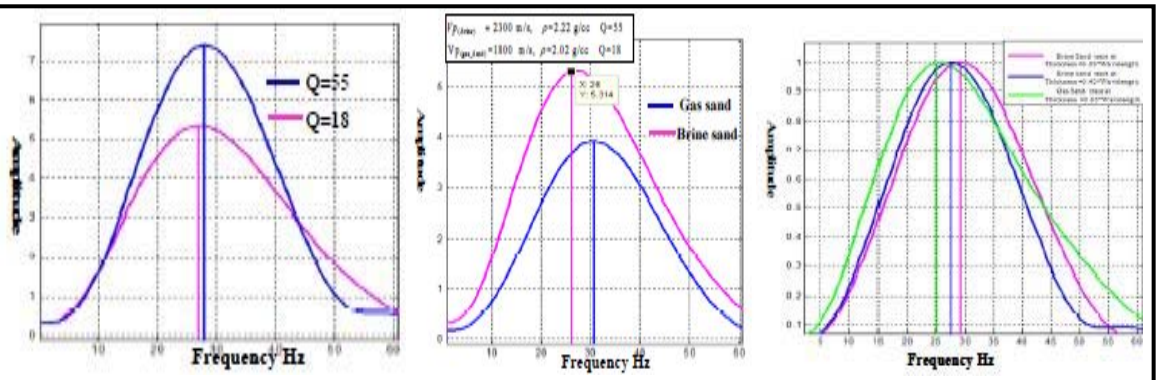

Figure 3.5: Shows the frequency response of attenuation, velocity and thickness respectively (left to right) at reservoir level. There is significant spectral shift due to velocity drop (Castagna et al., 2009).

Techniques

3.4 Continuous Wavelet Transform (CWT)

CWT method of signal transform was introduced by Morlet et al. (1982) and Goupillaud et al. (1985). It scales and translates the basis wavelet to produce series of wavelets which are convolved with the signal to produce time scale map (scalogram). The scale map is then transformed into time-frequency map, for analysis of the amplitudes and phase spectra of the individual frequencies (Castagna et al., 2006). CWT uses variable sized window length to analyze the wavelet of the signal which eliminates the fixed time window constraint of STFT (Okaya et al., 1995). As the size of the bandpass (window length) increases, the center frequency increases (Morlet et al., 1982). If we define a wavelet as a function $\psi(t) \xi R$, where $\psi(t)$ is continuous in both time and frequency domain, the scaling and translation of this basis wavelet $\psi(t)$ generate series of wavelets:

$$\psi_{(a,b)}(t) = \frac{1}{\sqrt{a}} \psi\left(\frac{t-b}{a}\right) \qquad (2)$$

where a and b are scale and translation parameter respectively. CWT of signal $f(t)$ with respect to wavelet $\psi(t)$ is given as:

$$CWT_{(a,b)} = \frac{1}{\sqrt{a}} \int_{-\infty}^{\infty} f(t)\psi^*(\frac{t-b}{a})dt \qquad (3)$$

where $*$ represents a complex conjugate and $CWT_{(a,b)}$ is time-scale map. To test the invertibility of CWT, (that is reconstruct the original signal), $f(t)$ from CWT. The Inverse Continuous Wavelet Transform (ICWT) gives:

$$f(t) = \int_{0}^{\infty} \int_{-\infty}^{\infty} \frac{1}{a^2} CWT_{(a,b)} \frac{1}{\sqrt{a}} \Psi(\frac{t-b}{a})dbda \qquad (4)$$

$\Psi(t)$ is the dual function of $\psi(t)$ and should satisfy admissibility condition (Morlet et al., 1982).

$$C_\psi = \int_{-\infty}^{\infty} \frac{|\Psi(w)|^2}{w} dw < \infty \qquad (5)$$

where C_ψ is the admissibility constant, and Ψ is the Fourier transform of ψ. For a successful inverse transform, the admissibility constant must satisfy $0 < C_\psi < +\infty$. Goupillaud et al. (1985) states the admissibility conditions that must be satisfied by the basis wavelet. These conditions are stated as follows:

(i) The wavelet must be absolutely integrable and square integrable (Okaya et al., 1995).

$$\int \psi(t)dt < \infty \text{ and } \int |\psi(t)|^2 dt < \infty$$

(ii) The wavelet must be band limited with zero mean (Okaya et al., 1995).

$$\int \left| \frac{\Psi(w)}{w} \right| dw < \infty.$$

Morlet wavelet as formulated by Goupillaud et al. (1985) satisfies the conditions above. Morlet wavelet is given as

$$\psi(t) = \ell^{jvt} \ell^{-\frac{t^2}{2}}.$$

The parameter v allows tradeoff between time and frequency resolutions. The constraint $v > 5$ is applied to prevent limitations with Morlet wavelet at high temporal resolution. Other wavelets that meet the admissibility conditions include: a vibroseis correlated wavelet, and an uncorrelated linear or nonlinear sweep but they are not as desirable as Morlet wavelet due to inherent ringiness (Okaya et al., 1995). The scale and the wavelet functions are the essential functions that define a wavelet. The scale factor a, either dilates or compresses a signal. It is responsible for the coverage of the spectrum of the wavelet, at a high value of a, the wavelet is compressed and the time resolution increases and at low value of a, the wavelet dilates and the time resolution decreases (Sinha et al., 2005). Figure 3.6 shows Morlet wavelet at different scales.

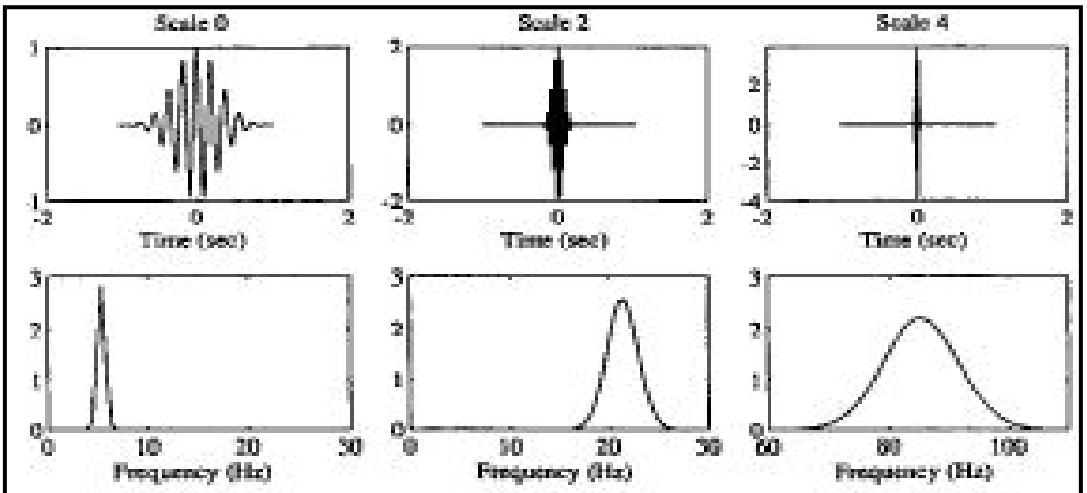

Figure 3.6: Morlet wavelet at different scales (Okaya et al., 1995).

3.5 Discrete Fourier Transform

DFT is a transform of a discrete time domain series into frequency domain (Okaya et al., 1992). The input function is usually a sequence of finite set of evenly spaced time sample whose non-zero values have limited durations. This function is usually a segment of an infinite length periodic signal (Goupillaud et al., 1985). If this is not true, a window function is introduced to enhance the spectrum artifact. The Inverse Discrete Fourier Transform (IDFT) cannot reconstruct the entire length of the original time domain signal but it reproduces the analyzed finite segment (Mallat et al., 1989). DFT is most often computed from Fast Fourier Transform (FFT) algorithms which reduce the running speed of the FFT. DFT computation from FFT algorithm is of the N^2 operation for transformation of an N-point sequence (Chambers et al., 1993). The transformation of a series of complex numbers $x_0.....,....x_{N-1}$ using DFT is given by:

$$X_D = \sum_{n=0}^{N-1} x_n \ell^{\frac{-2\pi i}{N} kn} \qquad (6)$$

where X_D is the amplitude and phase spectra of the sinusoidal components of the input sample x_n. In polar form, the amplitude and phase spectra can be expressed in terms of the complex modulus and argument of X_D,

$$\Phi_D = \arctan(I_m(X_D)/R_e(X_D)$$

where R_e and I_m are the real and imaginary components of X_D respectively. The Inverse Discrete Fourier Transform (IDFT) is given as:

$$X_n = \frac{1}{N}\sum_{D=0}^{N-1} X_D . \ell^{\frac{-2\pi kn}{N}} \quad . \qquad (7)$$

The above equation shows how to reconstruct the sampled function x_n by summing the sinusoidal components of equation (7) with frequency of $\frac{k}{N}$ cycles per sample. The vector $\ell^{\frac{2\pi ikn}{N}}$ forms the basis of the time series (Chambers et al., 1993). Transforming a time domain signal into frequency domain introduces aliasing which can be avoided if the Nquist frequency is higher than the maximum frequency component (Chambers et al., 1993). The analyzing window also influences the DFT resolution in that using a window length that is too short smears energy across bandwidth beyond the band of the original seismic data. Using a window length that is too long causes interference between non isolated reflections within the analysis window. This effect degrades the temporal resolution (Castagna et al., 2003).

3.6 Constrained Lease Squares Spectral Analysis (CLSSA).

CLSSA is a weighted least square constrained algorithm of spectral decomposition (Puryear et

al., 2012).The forward problem is given as:

$$FM = d \qquad (8)$$

where F is the kernel matrix with complex sinusoidal basis, M is the model parameter (desired spectral decomposition coefficients) and d is the window segment of the complex seismic trace. Since d is a complex trace, it can be expressed as:

$$d = d_r + id \qquad (9)$$

where d_r the real seismic traces and id is the Hilbert transform of the trace.

F is a complex sinusoid with length defined by the length of the analyzing window in time domain. F can be represented as:

$$F(\theta) = Cos\theta + iSin\theta \qquad (10)$$

where θ is given as $2\pi ft$, f is the discrete frequency and t is the discrete time window. Inj matrix, columns in F represent the number of frequencies and rows in F are the number of samples in the time window. Solving equation (8), the Least Mean Square Error (LMSE) solution is given as:

$$M = (F^* F)^{-1} F^* d \qquad (11)$$

where * is the complex conjugate transpose, if the sinusoids are uncorrelated, F*F=1 which reduces equation (11) to

$$M = F^* d\,. \qquad (12)$$

To have a unique solution, equation (8) is constrained with diagonal matrices. W_m and W_d. W_m is the model weighted matrix (Puryear C., 2012) given by:

$$W_m = G(K\Delta f) \qquad (13)$$

where $G(K\Delta f)$ is the frequency panel of the windowed spectrum. According to Portniaguine et al., (2004) writing the analytical Lagrange solution to the well-posed minimization of the Tikhonov parameter function gives:

$$M_w = F_w^*(F_w F_w^* + \alpha I)^{-1} W_d d. \qquad (15)$$

Using Gaussian elimination, the above equation is computed. Where F_w is a weighted quantity and M_d is diagonal matrix. (Interested reader is referred to Puryear , 2012).

Chapter Four

4.0 RESULTS AND DISCUSSION

4.1 Direct Hydrocarbon Detection

Spectral decomposition has a useful application to hydrocarbon detection, (e.g Castagna et al., 2003, Wei et al., 2011). The utility of spectral decomposition as hydrocarbon indicators is based on the fact that low frequency shadows are commonly observed beneath gas-charged reservoirs. These low frequency shadows are delineated as anomalous high amplitudes at low frequencies on iso-frequency sections, which gradually disappear at higher frequencies.

The approach adopted in this research involves interpreting seismic horizons that corresponds to hydrocarbon reservoirs. The next step is to transform the seismic volume into iso frequency volumes using the spectral decomposition techniques discussed earlier (sections 3.4, 3.5, and 3.6). To inspect for hydrocarbon detection, horizon slices that correspond to the hydrocarbon reservoirs are extracted from the various frequency volumes to produce spectral horizon maps. These maps are visually inspected for amplitude variations that are diagnostic of hydrocarbon in the reservoir.

Figure 4.1 shows the seismic section with yellow circle highlighting the Mississippian limestone (gas-charged reservoir) and black circle indicating the location of the Thirtyone Formation (gas reservoir).

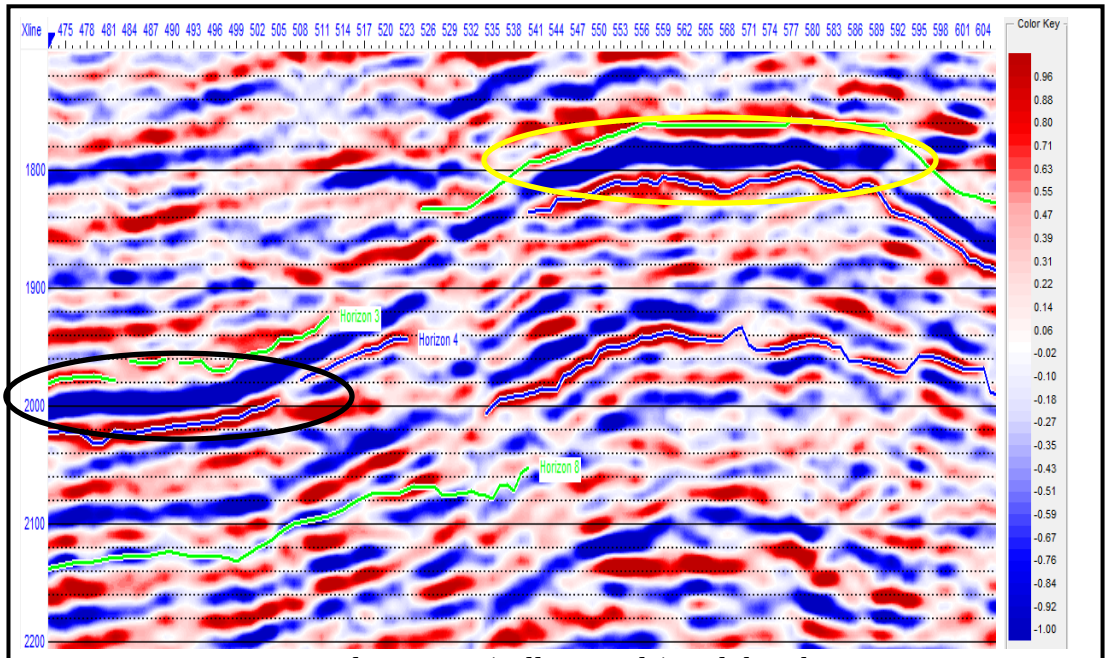

Figure 4.1: Mississippian limestone (yellow circle) and the Thirtyone Formation (black circle) on vertical seismic section.

Figure 4.2a is a DFT frequency volume at 25 Hz showing low frequency shadows indicated by black arrows. These low frequency shadows were observed beneath the Mississippian limestone and the Fusselman Formation. The Mississippian is approximately 30 m in thickness and the Fusselman Formation is about 25 m thick. At 65Hz (figure 4.2b), DFT preferentially illuminate the reservoirs with no background energy around the gas reservoirs. CLSSA also shows the high energy low frequency shadow beneath the reservoirs at 20Hz (figure 4.3a) and at 30Hz (figure 4.3b), the high energy low frequency shadows have been attenuated. This validates the newly developed CLSSA as a good hydrocarbon detection technique. CWT also identifies high energy low frequency shadows on the frequency volume at 25Hz (figure 4.4a) and at 73Hz (figure

4.4b), the shadows were attenuated. There is preferential illumination of the reservoirs are preferentially illuminated with little background energy on the frequency volume.

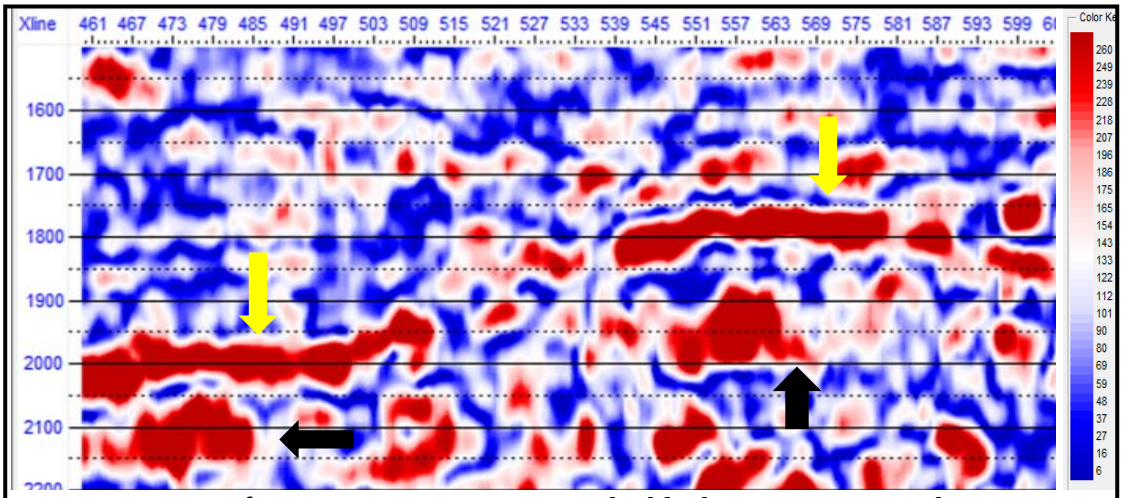

Figure 4.2a: DFT frequency section at 25 Hz, the black arrows point to the positions of the low frequency shadow and the yellow arrows point to the top of the reservoirs.

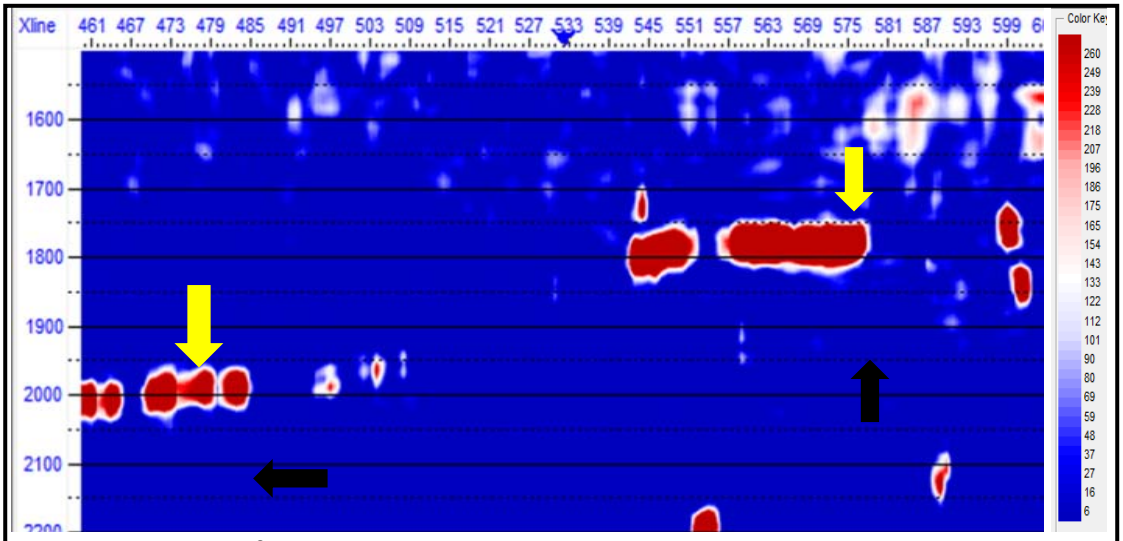

Figure 4.2b: DFT frequency section at 65 Hz, yellow arrows point to the reservoir location and the black arrow poing to the position of the shadows. Notice the shadows are gone (black arrows).

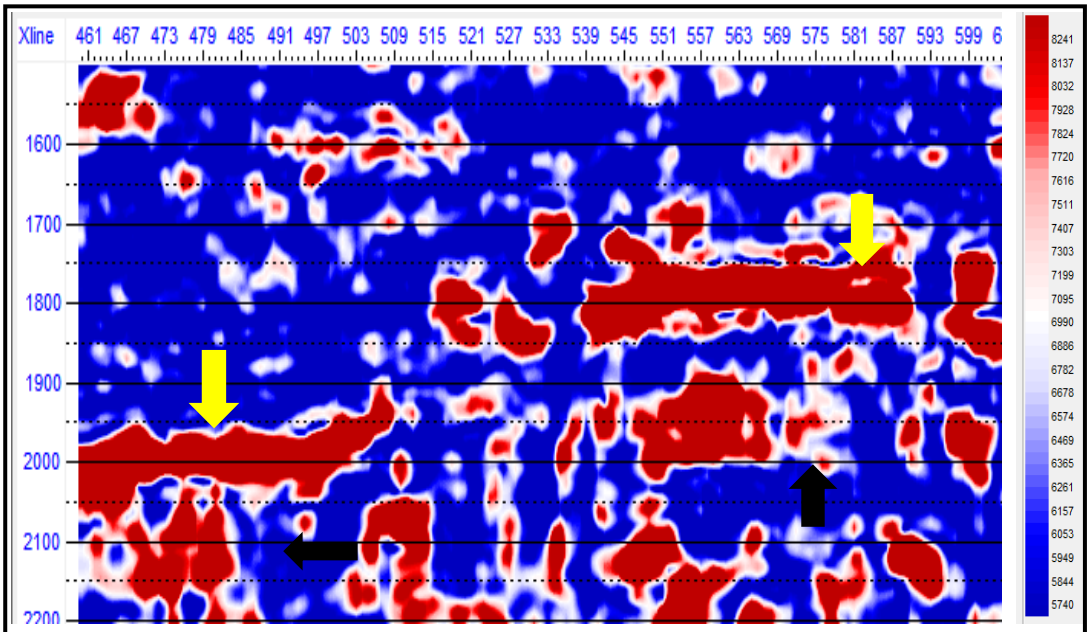

Figure 4.3a: CLSSA at 20 Hz, black arrow point to the shadows and the reservoirs locations are identify by yellow arrows.

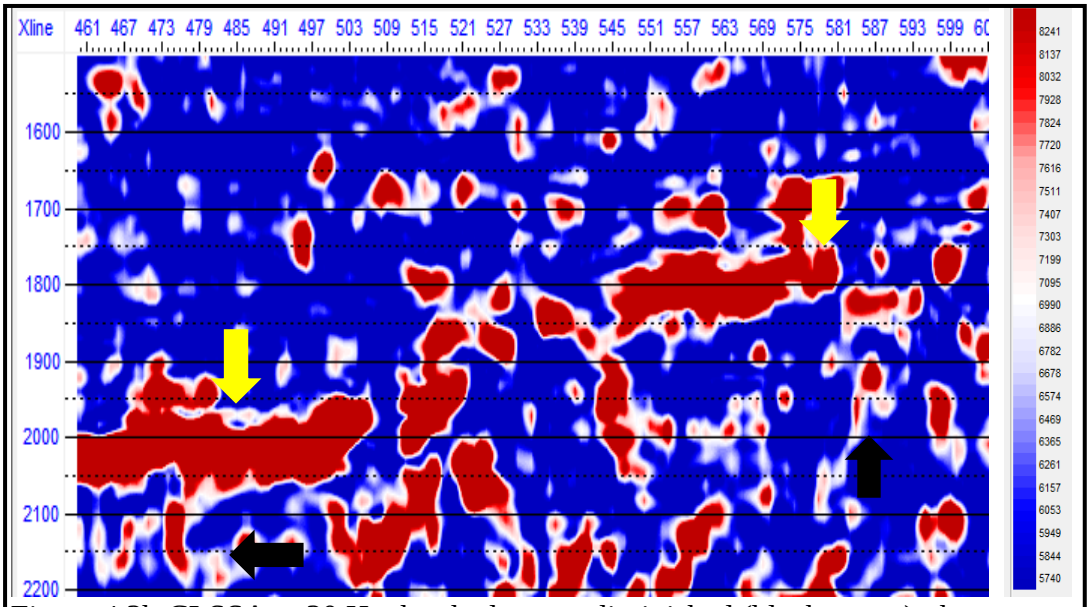

Figure 4.3b:CLSSA at 30 Hz the shadow are diminished (black arrow), the Yellow arrows pointing to the top of the reservoir.

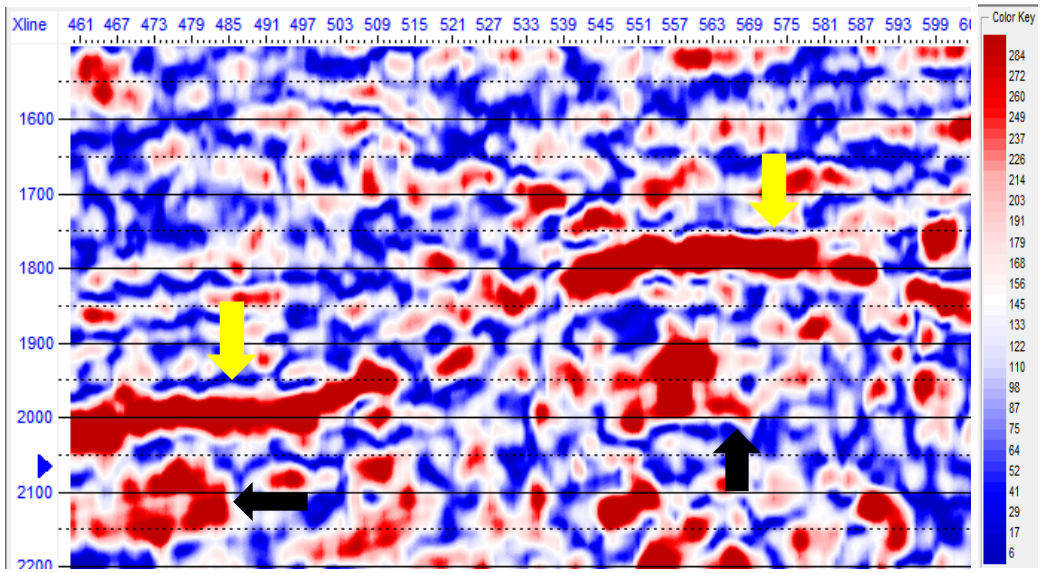

Figure 4.4a: CWT at 25 Hz identifies the shadows (black aroows) and reservoirs (yellow arrows).

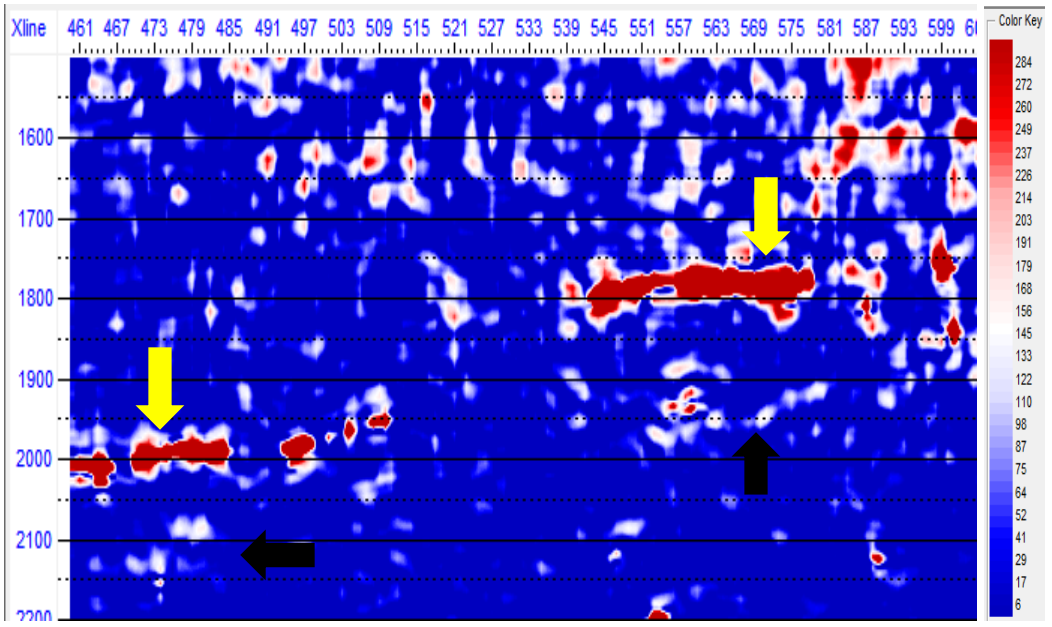

Figure 4.4b: CWT at 73, there is preferetcial illumination of the reservoirs, the shadows are diminished (black arrows)

Figure (4.5a) is an amplitude map obtained by taking a time slice at 1740 ms (20 ms above the Mississippian limestone) through the 25 Hz DFT volume. Figure (4.5b) is a time slice at 1950 ms extracted from the same 25 Hz DFT volume across the low frequency shadow. The reservoir locations are highlighted in black circles. The 25 Hz frequency volume shows high spectral energy at the location of the low frequency shadow (1950 ms), which is absent in the 1740 ms time slice indicating that the energy is localized around the low frequency shadow.

Figure 4.6 is the same time slices (1740 ms and 1950 ms) extracted from a higher frequency volume (65 Hz). The low frequency shadow does not show anomalous high spectral energy at this higher frequency, suggesting that the anomalous energy is only observed at low frequencies. This observation is consistent with the definition of low frequency shadow

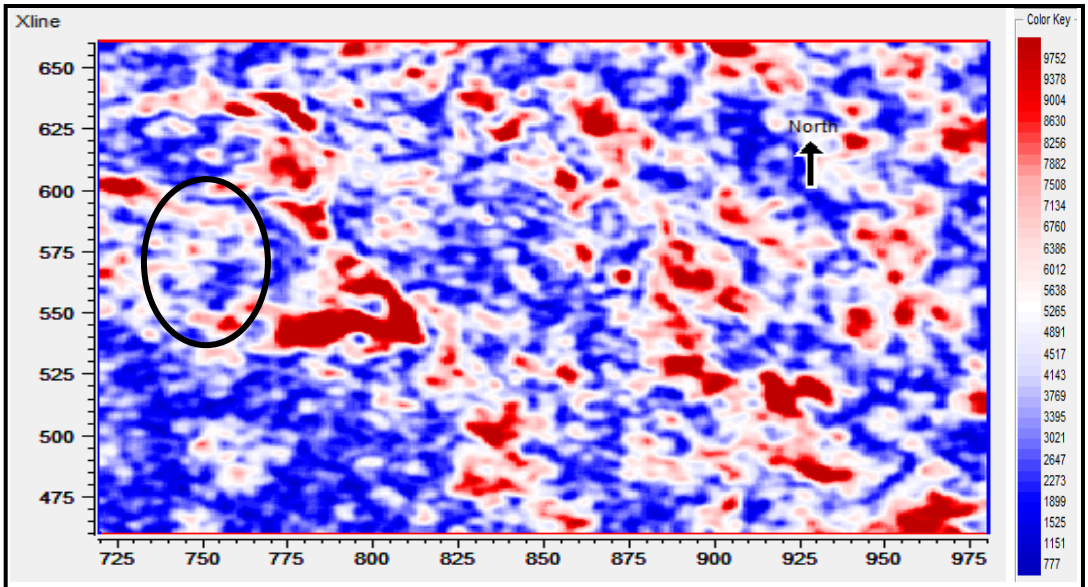

Figure 4.5a: Amplitude extraction on 25Hz frequency section at 20 ms above the reservoir. The reservoir location is indicated by black circle. Note the low energy at the reservoir and beneath the reservoir.

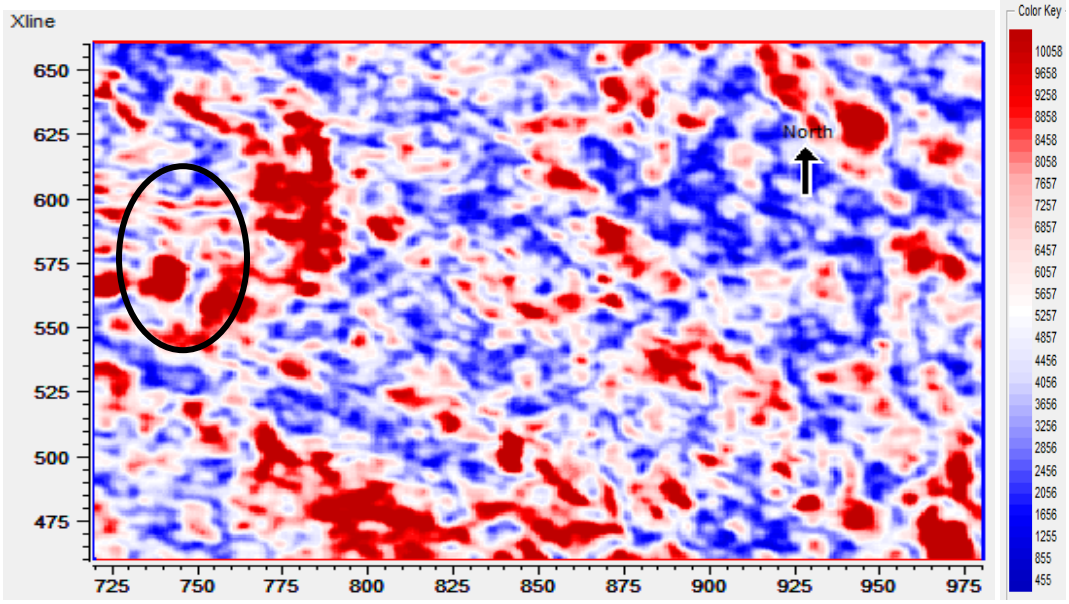

Figure 4.5b: Amplitude extraction on 25Hz section at the shadow. Notice the high energy beneath the reservoir.

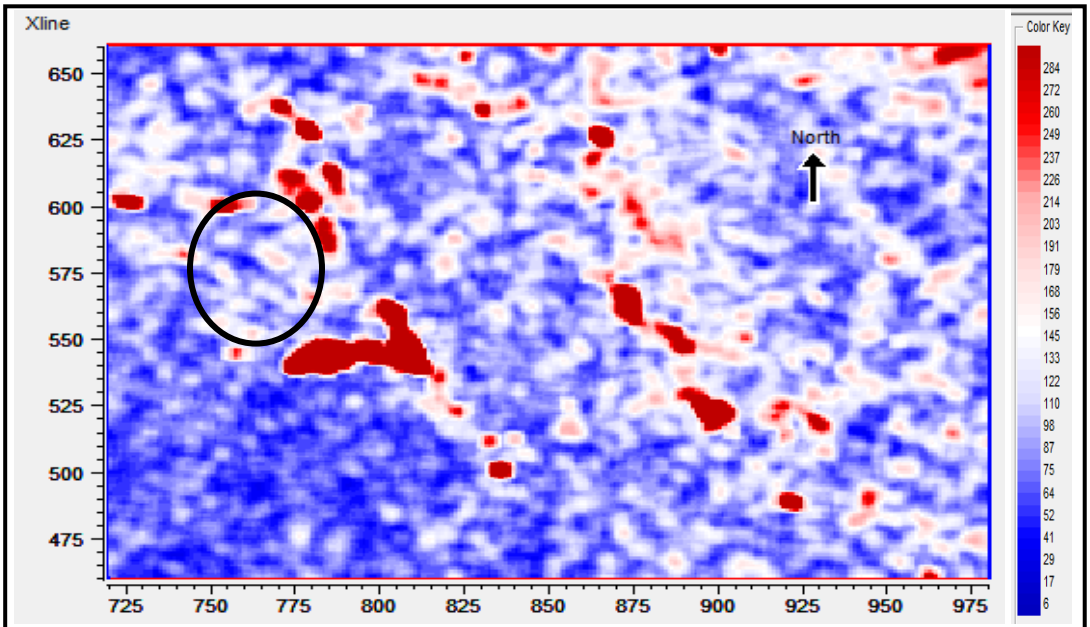

Figure 4.6a: Amplitude extraction on 65Hz frequency cube at 20 ms above the reservoir. Notice the higher energy beneath the reservoir compare with the amplitude extraction on the shadow (figure 4.6b)

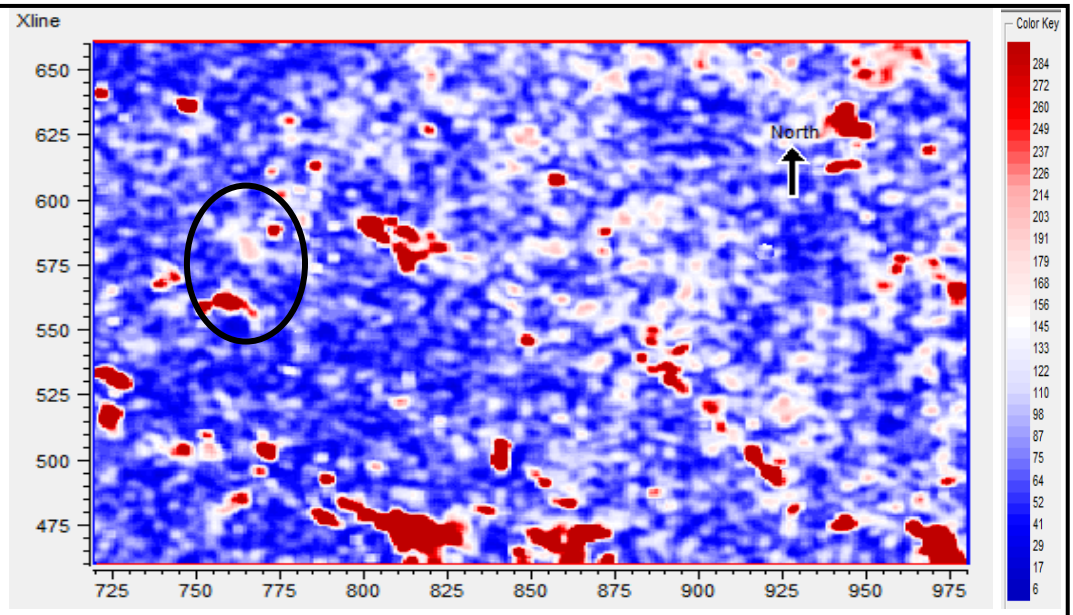

Figure 4.6b: Amplitude extraction on 65Hz section at the low frequency shadow. Note the low energy beneath the reservoir conforming to low frequency shadow diminishing at high frequency.

4.2 Structure Interpretation

This study is extended to test the resolution of the various techniques in structural delineation. A meandering river on the Straton field exactly the same studied by Sinha et al., 2005, was used to validate the power of the techniques used. A channel was picked on the seismic section as shown in figure 4.7, the black arrow points to the location of the channel and the yellow line is the picked horizon. The RMS amplitude of the horizon is shown in figure 4.8 with black arrows pointing to the channel features. The horizon is extracted and CLSSA, DFT, and CWT algorithms were applied to further enhance the visibility of the features.

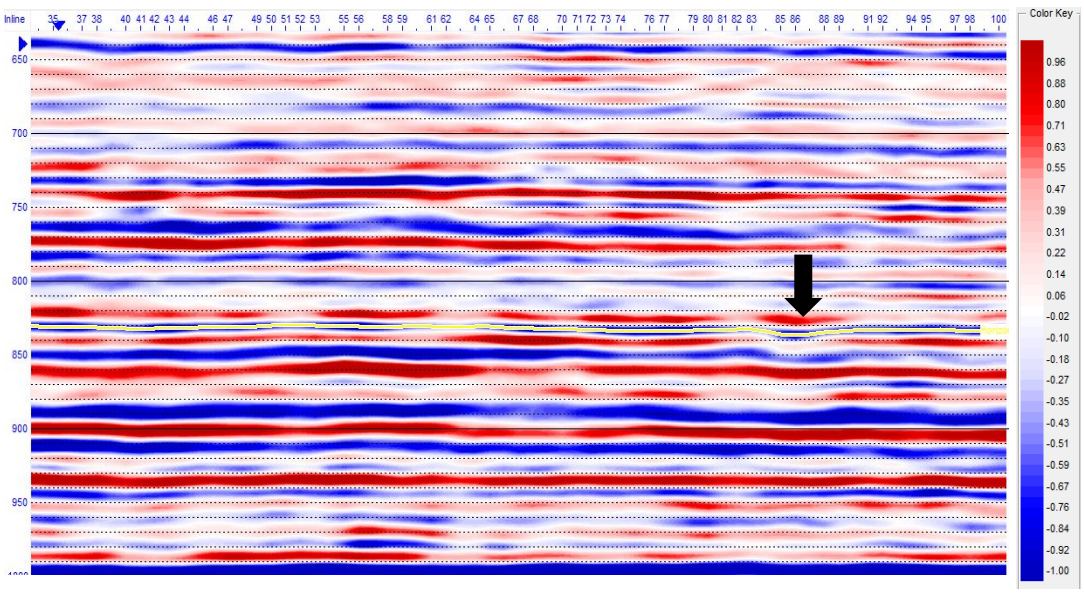

Figure 4.7: Show the vertical seismic section with the location of the channel indicated with black arrow and the horizon pick in yellow.

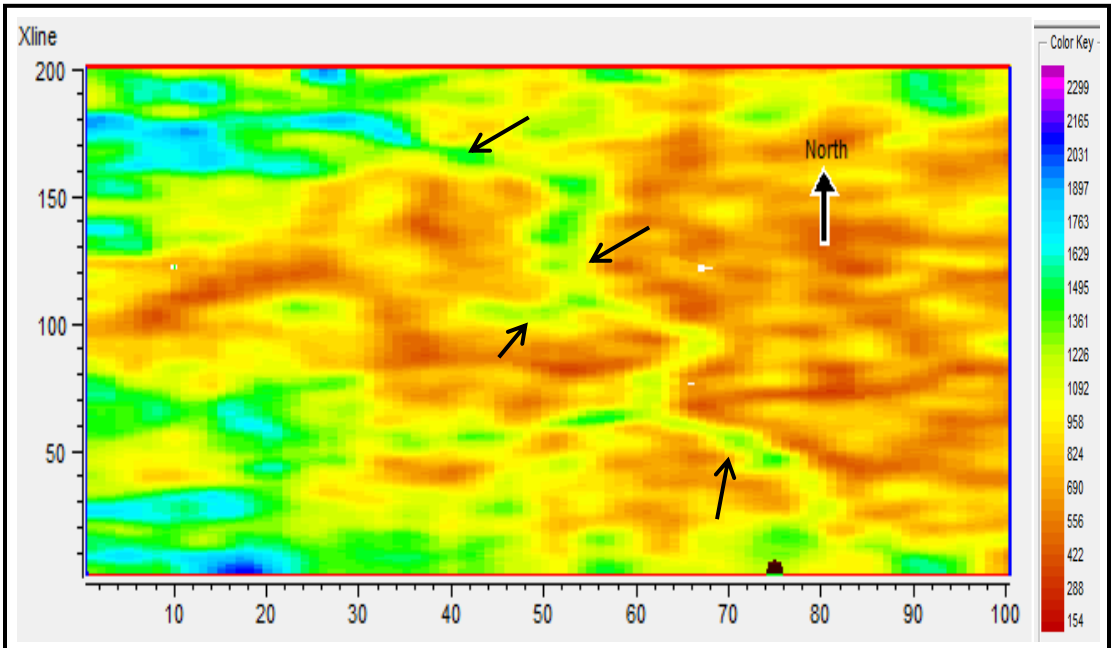

Figure 4.8: RMS Amplitude map of the horizon, the arrows are pointing to the channel features on the map.

CLSSA at 29Hz delineates the channel and further enhances it extent along the branching which was not seen on the amplitude map. Yellow arrows show the extension of the channel that was not seen on the amplitude map on the southwestern and northwestern part of the horizon spectral decomposition map (figure) 4.9. DFT horizon spectral decomposition with 40 ms analyzing window at 23Hz highlights the channel feature and also extends the branching beyond what was shown on the amplitude map, yellows arrows on figure 4.10 show the channel branching delineated by DFT but it suffers from background energy interference which blurs the continuity of the channel extent on the southwestern and northwestern part of the map. CWT at 57Hz delineates the channel feature (figure 4.11) but this method at some point has discontinuity in the lateral extent of the feature, it gives the least result in terms of delineating structures.

CLSSA gives the best result as it emphasized the channel more than it was highlighted on the RMS amplitude map.

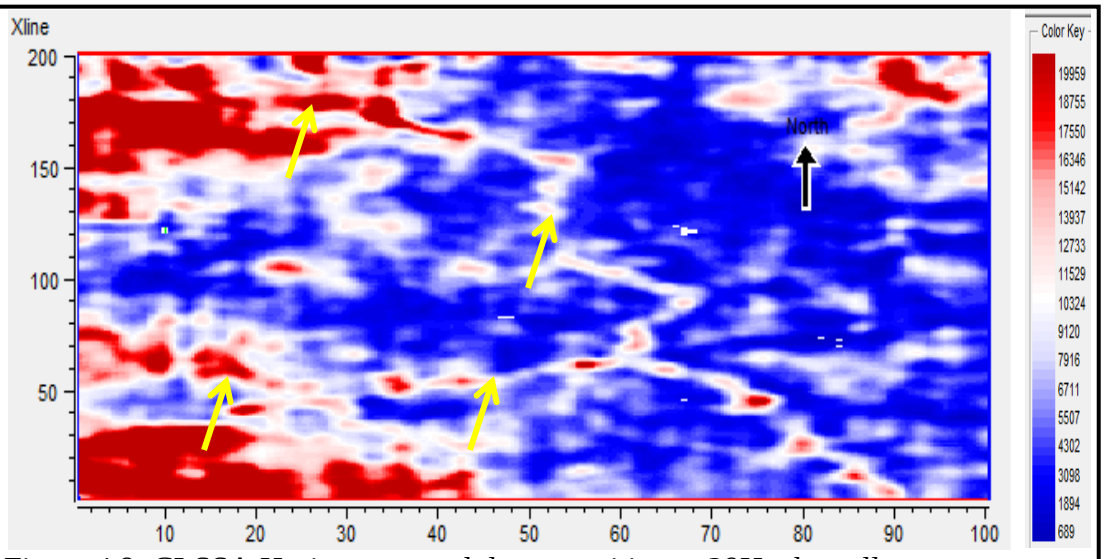

Figure 4.9: CLSSA Horizon spectral decomposition at 29Hz the yellow arrows indicate the extension of the channel seen on CLSSA that are not visible on amplitude map.

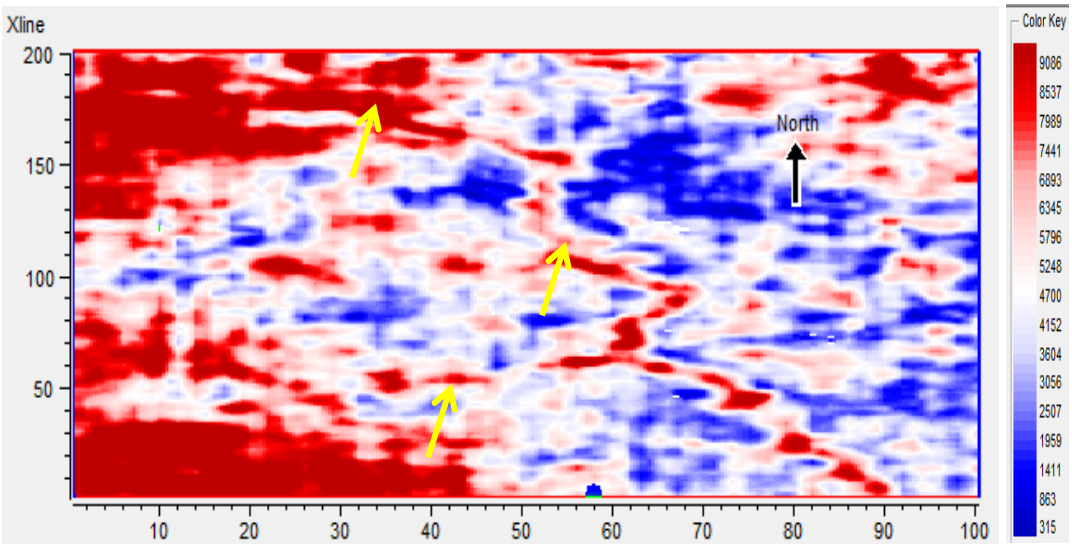

Figure 4.10: DFT Horizon spectral decomposition at 23Hz the yellow arrows indicate the extension of the channel seen on DFT that are not visible on amplitude map.

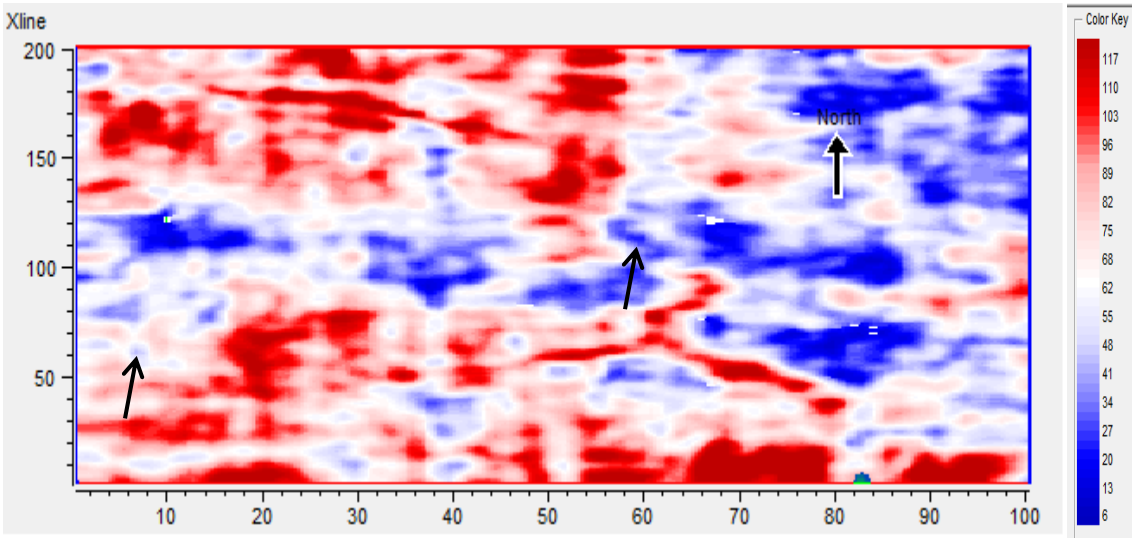

Figure 4.11: CWT horizon spectral decomposition at 57Hz, black arrows show the point of discontinuities of the channel on the map.

4.3 FREQUENCY GATHER

Frequency gather was computed on synthetic traces from two wells, Well 37 and Well 46. This exercise is aimed at comparing the resolution of the techniques on a trace by trace basis. It was observed that CLSSA has a better resolution of separating events on seismic trace. It resolve side lobe distinctively and has minimal notches compared with other methods. DFT also did a good job of separating events on the traces, but it has the limitation of side lobe effects and notches were observed on the DFT frequency gather. CWT has the least resolution of the events, typical of CWT poor time resolution at low frequencies which is the major limitation of the technique on a seismic section with low frequency content. The black box in figure 4.12 shows two events that are closely spaced in time, CLSSA resolves these events distinctively without side lobe effects or interference pattern. DFT also separate the events but side lobe effect blurs the

separation while CWT could not separate the events in time. Figure 4.13 shows the position of the reservoir in black arrow, Although, CLSSA and DFT resolves these events, the time resolution of the CLSSA is better than DFT.

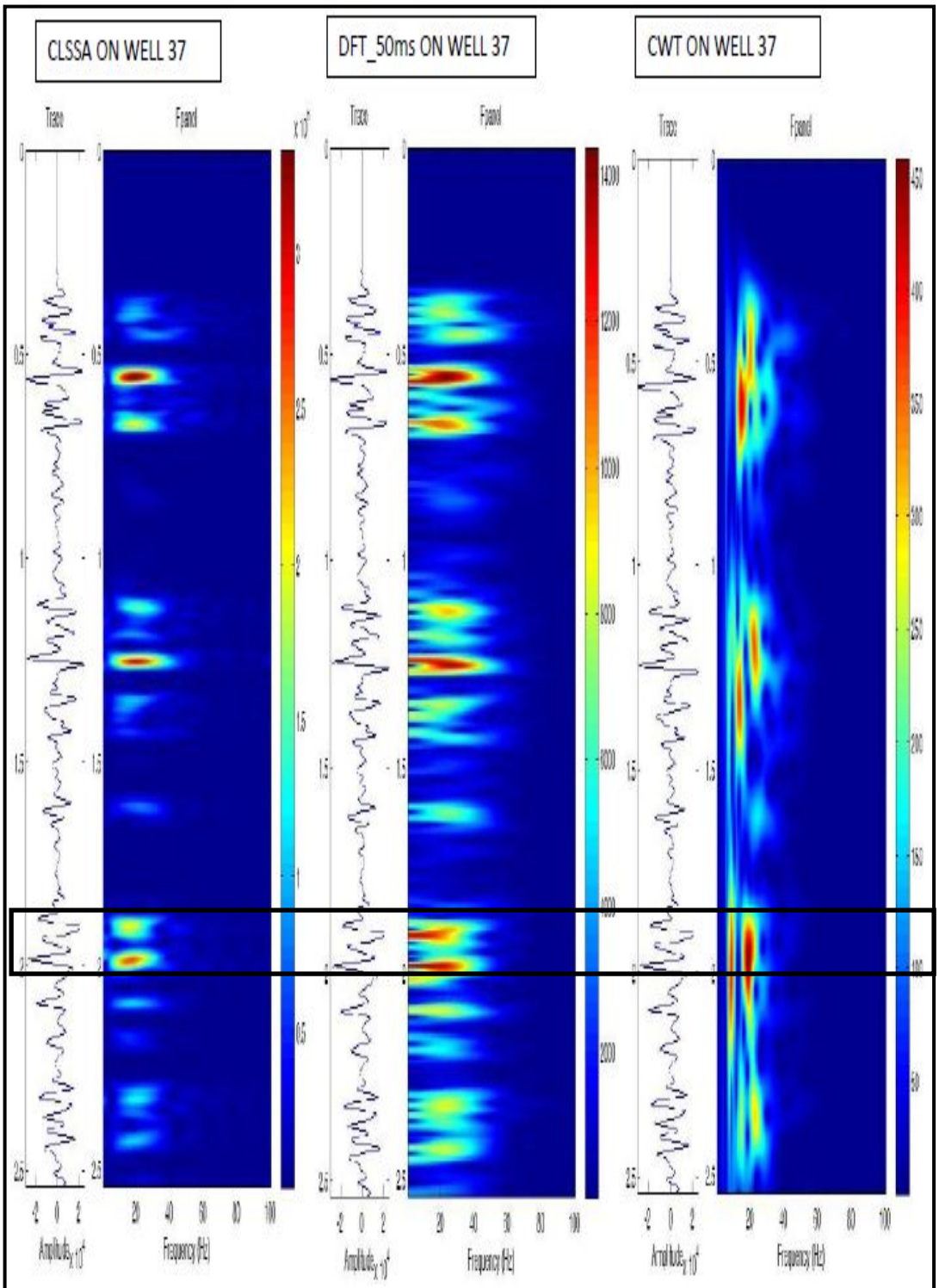

Figure 4.12a: Comparison of frequency gathers on synthetic trace from Well 37

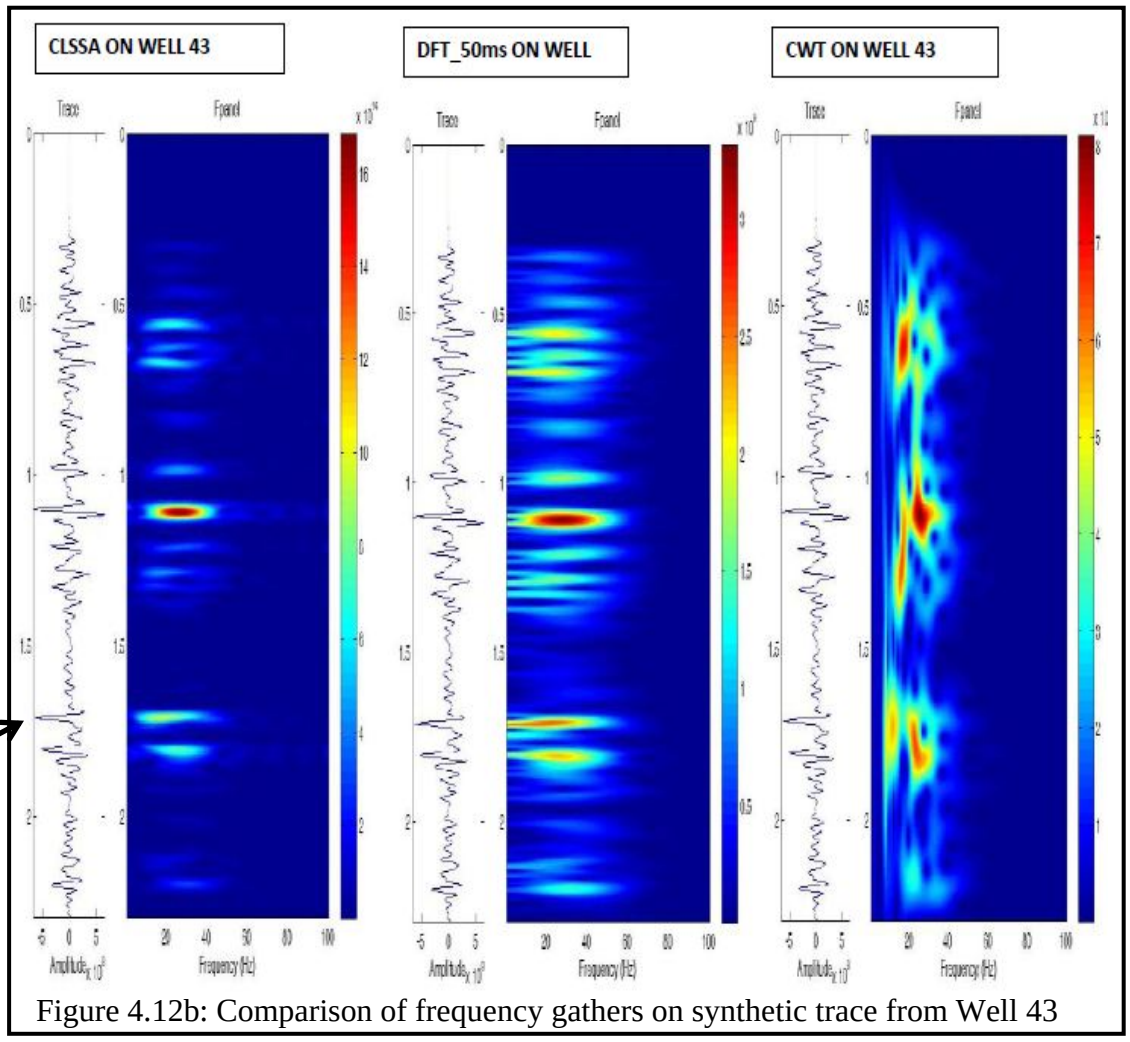

Figure 4.12b: Comparison of frequency gathers on synthetic trace from Well 43

Chapter 5

5.0 Conclusion

Three spectral decomposition techniques, namely, DFT, CWT, and CLSSA were applied to a 3D seismic data from the Waha Fields, West Texas. These spectral decomposition techniques were accessed for their time-frequency resolution and effectiveness in delineating subtle reservoir features on seismic horizons. The amplitude spectra for these techniques were computed for a single seismic trace and for a seismic horizon. The results show CLSSA to have improved time-frequency resolution over the DFT and CWT. Spectral and temporal smearing that degrades the DFT and CWT spectrum are greatly reduced in the CLSSA spectrum. CLSSA is found to give better spectral characteristics of the original seismic and thus emphasizing subtle features not observed on the original seismic data.

A second study to investigate the utility of these techniques as direct hydrocarbon indicators was also presented. The result shows that DFT is best for hydrocarbon detection because the low frequency shadows were well localized and reservoirs were preferentially illuminated at high frequency. But CWT and CLSSA also identified the reservoirs in the study area. This research validates the recently developed CLSSA is a good structural delineation and hydrocarbon detection technique.

6.0 References.

Asquith, G. and Gibson C. 1982 Basic well log analysis for geologist: AAPG, Tulsa Oklahoma. Series 3, 41-100.

Burnett, M., J. P. Castagna, E. Méndez Hernández, G. Ziga Rodríguez, L. Figón García, J. Martínez Vázquez, M. Téllez Avilés, and R. Vila Villaseñor, 2003, Application of spectral decomposition to gas basins in Mexico: The Leading Edge, 22, 1130-1134.

Castagna, J.P., Sun, S. and Siegfried, R.W. 2003 Instantaneous spectral analysis: detection of low-frequency shadows associated with hydrocarbons. *The Leading Edge*, 22, 120-127.

Castagna, J.P., Shenghong T., and Puryear C., 2009 Local frequency as a direct hydrocarbon indicator. SEG Extended Abstracts 28, 2160-2164.

Chambers E.. Michael J.R., and Hung V. 1993 Computing the Fourier transform in geophysics with the transform decomposition DFT: Geophysics 58, No.11, 1707-1709

Chopra, S., Castagna, J.P. and Portniaguine, O. 2006 Seismic resolution and thin-bed reflectivity inversion. *CSEG Recorder*, 31, 19-25.

Chopra, S., Castagna, J.P. and Portniaguine, O. 2006 Thin- bed reflectivity inversion SEG/New Orleans 2006 Annual Meeting Expanded Abstract, 2057-2061.

Chopra, S., Castagna, J.P., Yong Xu and Rainer Tonn. 2007 Thin- bed reflectivity inversion and seismic interpretation. SEG/San Antonio 2007 Annual Meeting Expanded Abstract, 1923-1927.

Comer, J. B., 1991, Stratigraphic analysis of the Upper Devonian Woodford Formation, Permian Basin, West Texas and southeastern New Mexico: The University of Texas at Austin, Bureau of Economic Geology Report of Investigations No. 201, 63 p.

Ebrom, D., 2006, The low-frequency gas shadow on seismic sections: The Leading Edge, **23**, Issue 8, 772.

Ewing, T. E., 1991, The tectonic framework of Texas: text to accompany "The Tectonic Map of Texas": Bureau of Economic Geology, The University of Texas at Austin, 36 p.

Fahmy, W. A., G. Matteucci, D. Butters, and J. Zhang, 2005, Successful application of spectral decomposition technology toward drilling of a key offshore development well: 75th Annual International Meeting of the Society of Exploration Geophysicists, Expanded Abstracts, 262-264.

Gao, D., 2007, 3D seismic interpretation, unpublished lecture notes.

Goupillaud, P., Grossmann, A., and Morlet, J., 1985, Cycle octave and related transforms in seismic signal analysis:, *in* IEEE Geoexploration: Elsevier Science Publishers B.V., 23, 85-102.

Hardage, B. A., Major, R. P., Hentz, T. F., eds., 1998, Integrated strategies for carbonate reservoir reserve growth: an example from the Ellenburger Group, Permian Basin, West Texas: The University of Texas at Austin, Bureau of Economic Geology project report prepared for the U.S. Department of Energy and Gas Research Institute, variously paginated.

Hardage, B. A., Simmons, J. L., Jr., Lancaster, D. E., Elphick, R. Y., Edson, R. D., and Carr, D. L., 1996, Boonsville 3-D seismic data set: The University of Texas at Austin, Bureau of Economic Geology.

Holtz, M. H., and Garrett, C. M., Jr., 1997, Play analysis and resource assessment of Texas State Lands, *in* Major, R. P., ed., Oil and gas on Texas State Lands: an assessment of the resource and characterization of type reservoirs: The University of Texas at Austin, Bureau of Economic Geology Report of Investigations No. 241, 1-30.

Holtz, M. H., and Kerans, Charles, 1992, Characterization and categorization of West Texas Ellenburger reservoirs, *in* Candelaria, M. P., and Reed, C. L., eds., Paleokarst, karst-related diagenesis, and reservoir development: examples from Ordovician-Devonian age strata of West Texas and the Mid-Continent: Permian Basin SEPM Publication 92-33, 45-58.

Jones, T. S., 1953, Stratigraphy of the Permian Basin of West Texas: West Texas Geological Society, 57 p.

Kerans, Charles, 1988, Karst-controlled reservoir heterogeneity in Ellenburger Group carbonates of West Texas: American Association of Petroleum Geologists Bulletin, 72, (10), 1160-1183.

Kerans, Charles, 1990, Depositional systems and karst geology of the Ellenburger Group (Lower Ordovician), subsurface West Texas: The University of Texas at Austin, Bureau of Economic Geology Report of Investigations No. 193, 63 p.

Kupecz, J. A., and Land, L. S., 1991, Late-stage dolomitization of the Lower Ordovician Ellenburger Group, West Texas: Journal of Sedimentary Petrology, 61, (4), 551-574.

Levey, R. A., Hardage, B. A., Edson, R. D., Jr., and Pendleton, V. M., 1994, 3-D seismic and well log data set: fluvial reservoir systems-Stratton field, South Texas: The University of Texas at Austin, Bureau of Economic Geology.

Loucks, R. G., and Anderson, J. H., 1985, Depositional facies, diagenetic terranes, and porosity development in Lower Ordovician Ellenburger dolomite, Puckett field, West Texas, in Roel, P. O., and Choquette, P. W., Carbonate petroleum reservoirs: New York, Springer-Verlag, 21-37.

Loucks, R. G., and Handford, C. R., 1992, Origin and recognition of fractures, breccias, and sediment fills in paleocave-reservoir networks, in Candelaria, M. P., and Reed, C. L., eds., Paleokarst, karst-related diagenesis, and reservoir development: examples from Ordovician-Devonian age strata of West Texas and the Mid-Continent: Permian Basin SEPM Publication 92-33, 31-44.

Lucia, F. J., 1995, Lower Paleozoic cavern development, collapse, and dolomitization, Franklin Mountains, El Paso, Texas, *in* Budd, D. A., Saller, A. H., and Harris, P. M., eds., Unconformities and porosity in carbonate strata: American Association of Petroleum Geologists Memoir 63, p. 279-300.

Mallat, S., 1989, A theory of multi resolution signal decomposition, the wavelet representation: IEEE Trans. Pattern analysis and intelligence, 14, 710-732.

Marfurt, K.J., and R. L. Kirlin, 2001, Narrow-band spectral analysis and thin-bed tuning: Geophysics, 66, 1274-1283.

Morlet, J., G. Arens, E. Fourgeau, and D. Giard, 1982, Wave propagation and sampling theory-Part II: sampling theory and complex waves: Geophysics, 47, 222-236

Okaya D. and Chakraborty A. 1995, Frequency-time decomposition of seismic data using wavelet-based methods. Geophysics, 60, (6), 1906-1916.

Okaya D. and Chakraborty A. 1992, Spectral properties of the earth's contribution to seismic resolution. Geophysics, 60, 241-251.

Partyka, G.A., Gridley, J. and Lopez, J. 1997 Processing and interpretational aspect of spectral decomposition. SEG Expanded Abstract, 16, 1055-1058.

Partyka, G.A., Gridley, J. and Lopez, J. 1999 Interpretational applica-tions of spectral decomposition in reservoir characterization. The Leading Edge, 18, 353-360.

Portniaguine, O. and J.P. Castagna 2005 Spectral inversion: Lessons from modeling and Boonesville case study. 75th SEG Annual Meeting. Expanded Abstracts, 1638-1641.

Puryear, C.I. and Castagna, J.P. 2008 Layer-thickness determination and stratigraphic interpretation using spectral inversion: theory and application. *Geophysics*, **73**, R37-R48.

Puryear, 2012 Constraint lease square spectral analysis. Unpublished PHd.Thesis, University of Houston, Dept. of Earth & Atmospheric Sciences.

Ruppel, S. C., 1989, Summary of Mississippian stratigraphy in north and north central Texas, *in* Mear, C. E., McNulty, C. L., and McNulty, M. E., eds., A symposium on the geology of Mississippian carbonates in north central Texas: Forth Worth Geological Society and Texas Christian University, p. 49-55.

Ruppel, S. C., and Holtz, M. H., 1994, Depositional and diagenetic facies patterns and reservoir development in Silurian and Devonian rocks of the Permian Basin: The University of Texas at Austin, Bureau of Economic Geology Report of Investigations No. 216, 89 p.

Ruppel, S. C., and Hovorka, S. D., 1995, Chert reservoir development in the Devonian Thirtyone Formation: Three Bar field, West Texas: The University of Texas at Austin, Bureau of Economic Geology Report of Investigations No. 230, 50 p.

Sinha, S., P. Routh, P. Anno, and J. P. Castagna, 2005, Spectral decomposition of seismic data with continuous-wavelet transform: Geophysics, 70, 19-25.

Taner, M.T., F. Koehler, and R. E. Sheriff, 1979, Complex seismic trace analysis: Geophysics, 44, 1041-1063.

Wright, W. F., 1979, Petroleum geology of the Permian Basin: West Texas Geological Society Publication No. 79-71, 98 p.

Wang, Y., 2007, Seismic time-frequency spectral decomposition by matching pursuit: Geophysics, 72, (1), 13–20.

Wei D., Xin W., and Gerard B., 2011, Least-squares migration of multisource data with a deblurring filter: Geophysics 76, 135-146

Widess, M. B., 1973, How thin is a thin bed: Geophysics, 38, 1176-1180.

Winkler, K., Nur, A., and Gladwin. M., 1979. Friction and seismic attenuation in rocks: Nature, 277, 528-531.

Winkler. K., and A. Nur, 1982, Seismic attenuation: Effects of pore fluids and frictional sliding: Geophysics, 47, 1–15.

Yandong, L., Xiandong Z., and Yan Z., 2011, High frequency anomalies in carbonate reservoir characterization using spectral decomposition: Geophysics, 76, 47-57